

Late Holocene structural style and seismicity of highly transpressional faults in southern Haiti

Jiannan Wang, Paul Mann, Robert R. Stewart

Department of Earth and Atmospheric Sciences, University of Houston, Houston, Texas, USA.

Key Points:

- First high-resolution sonar surveys of two actively deformed lakes in Haiti.
- High degree of regional, tectonic transpression is partitioned by *en echelon* thrust faults and associated folds adjacent to a major strike-slip, plate boundary fault.
- ~~Estimates of relative ages of deformation of major strike-slip faulting and *en echelon* thrusts from deformed and undeformed lake sediments.~~ 3D deformation model integrates patterns of 2010 coseismic uplift, aftershock distribution, and mapped geologic structures.

13 **Abstract**

14 The devastating 2010 Haiti earthquake (M_w 7.0) was caused by rupture of the Léogâne,
 15 blind, thrust fault located 5 km north of ~~the main, Caribbean-Gonâve one of the main~~
 16 ~~Northern Caribbean~~ plate boundary, a 1200 km-long, left-lateral, Enriquillo-Plantain Gar-
 17 den fault zone (EPGFZ). Unexpectedly, the EPGFZ ~~, which~~ remained largely quiescent
 18 or slightly reactivated during the 2010 earthquake, ~~although~~. ~~However, it still~~ formed a
 19 boundary between a coseismically uplifted lowland north of the EPGFZ and a subsided
 20 area in the highlands south of the fault. Here, we use high-resolution sonar data from two,
 21 Haitian lakes that straddle the EPGFZ and its northern flank to demonstrate the presence
 22 of a 10 – 15 km-wide, 120 km-long, late Holocene fold-thrust belt which deforms clas-
 23 tic, lowland basins along the northern edge of the EPGFZ. In the eastern part of the study
 24 area, sonar results from Lake Azuey show that the linear trace of the EPGFZ cutting the
 25 Holocene lake bed is more deeply buried and less active than the adjacent, newly discov-
 26 ered, northwest-striking, northeast-dipping Jimani thrust fault that is part of the adjacent
 27 ~~transpressional~~ ~~transpressional~~ belt of *en echelon* thrust-and-fold. This structural relation-
 28 ship between a less active EPGFZ and more recently active, transpression-related Jimani
 29 thrust is remarkably similar to the 2010 epicentral area 70 km to the west between the less
 30 active EPGFZ and seismogenic Léogâne thrust during the 2010 Haiti earthquake. In this
 31 complex transpressional zone, we propose that coseismic deformation alternates at recur-
 32 rence intervals of centuries between oblique, transpression-related structures (Léogâne,
 33 Jimani, and Trois Baies blind thrusts) and the main strike-slip, plate boundary fault zone
 34 (EPGFZ).

35 **1 Introduction and tectonic setting of the 2010 Haiti earthquake**

36 On January 12, 2010, a M_w 7.0 earthquake struck the densely populated, greater
 37 Port-au-Prince region of south-central Haiti and caused widespread destruction with over
 38 230,000 fatalities and an estimated 10 billion dollars damage [Prentice *et al.*, 2010; Bil-
 39 ham, 2010; Paultre *et al.*, 2013; Kocel *et al.*, 2016] (Figure 1). Multidisciplinary, geolog-
 40 ical and geophysical studies of the 2010 epicentral area of south-central Haiti ~~have been~~
 41 ~~done~~, including: 1) coseismic, coral reef uplift observation along a 50 km-long area of
 42 coastline in the epicentral region combined with fault modeling [Hayes *et al.*, 2010]; 2)
 43 coseismic, vertical ground motion from radar interferometry [Hashimoto *et al.*, 2011];
 44 3) high-resolution, surface-fault-trace mapping using Light Detection And Ranging (LI-

45 DAR) and targeted field studies [Cowgill *et al.*, 2012]; 4) Global Positioning System (GPS)
 46 and 2010 aftershock-based studies and modeling of pre-, syn-, and post-2010 earthquake
 47 crustal motions [Calais *et al.*, 2010; Nettles and Hjörleifsdóttir, 2010; Symithe *et al.*, 2013;
 48 Douilly *et al.*, 2013, 2015]; 5) ground-based studies of Holocene scarps including coseis-
 49 mic ground fractures and late Quaternary scarps of the EPGFZ that remained unaffected
 50 by 2010 fault breaks [Prentice *et al.*, 2010; Koehler and Mann, 2011; Rathje *et al.*, 2014;
 51 Saint Fleur *et al.*, 2015]; 6) ground-based, near-surface, geophysical surveys of buried
 52 faults activated during the 2010 earthquake [Kocel *et al.*, 2016]; 7) near-coast surveys of
 53 submarine extensions of faults active in 2010 [Hornbach *et al.*, 2010; Mercier de Lépinay
 54 *et al.*, 2011]; and 8) deepwater, marine surveys and coring to determine the recurrence in-
 55 terval of major earthquakes based on anomalous sedimentary deposits related to shaking
 56 and increased erosion [McHugh *et al.*, 2011].

57 The consensus from these previous, on- and offshore, multidisciplinary studies is
 58 that the 2010 earthquake ruptured two, previously unrecognized west- to northwest-striking
 59 thrust faults located 2 to 5 km north of the 1200 km-long, left-lateral, Enriquillo-Plantain
 60 Garden fault zone (EPGFZ) that forms a major, plate boundary between the Caribbean
 61 plate to the south and the Gonâve microplate to the north [Mann *et al.*, 1995; Calais *et al.*,
 62 2010; Benford *et al.*, 2012; Corbeau *et al.*, 2016] (Figure 1A, B). These two ~~thrust~~ thrust
 63 are separated by 6 km and include: 1) the subaerial, 8 km-long, blind, Léogâne thrust
 64 fault located 5 km north of the EPGFZ and trending at an angle of 8° to the EPGFZ [Calais
 65 *et al.*, 2010; Douilly *et al.*, 2013, 2015]; and 2) the submarine, 20 km-long Trois Baies
 66 thrust fault located 2 km north of the EPGFZ and trending at an angle of 20° [Mercier de
 67 Lépinay *et al.*, 2011; Symithe *et al.*, 2013] (Figure 1B, C).

68 Despite the proximity of the Léogâne and Trois Baies thrust to the neighboring
 69 EPGFZ, the EPGFZ remained largely ~~quiescently~~ quiescent and outside the zone of maxi-
 70 mum, coseismic uplift and ground shaking and aftershocks related to the 2010 earthquake
 71 [Nettles and Hjörleifsdóttir, 2010]. The centroid moment tensor (CMT) mechanism of the
 72 main 2010 shock shows a primarily strike-slip motion, with a small component of reverse
 73 motion, on a steeply north-dipping nodal plane [Nettles and Hjörleifsdóttir, 2010; Douilly
 74 *et al.*, 2013]. Finite element modeling [Douilly *et al.*, 2015] suggests that Léogâne fault
 75 buried beneath at least 1 km of overlying undeformed clastic sediment in the area north
 76 of the EPGFZ absorbed most of the energy of the ~~northwest-southeast~~ northwest-southeast
 77 compression along obliquely-striking, high-angle (21°-70° dipping) reverse fault planes,

78 leaving significantly increasing but ~~insufficient~~ ~~not enough~~ stress to trigger a 2010, coseis-
 79 mic slip on the adjacent EPGFZ 5 km to the south (Figure 1B). Previous GPS surveys ~~by~~
 80 ~~show~~ [Calais *et al.*, 2010, 2016] along this area of the EPGFZ display vectors at almost
 81 right angles to these obliquely-striking thrusts and consistent with their preferred reactiva-
 82 tion (Figure 1A, B).

83 Aftershock studies following the 2010 earthquake by Douilly *et al.* [2013, 2015]
 84 showed that the EPGFZ moved slightly at depth and acted as a 6 km-long, east-west and
 85 sub-vertical, connecting fault segment that transmitted seismogenic motion between the
 86 obliquely-trending, ~~south-dipping~~ ~~north-dipping~~, Léogâne fault in the east and the more
 87 obliquely-trending, ~~northeast-dipping~~ ~~southwest-dipping~~ Trois Baies fault in the west (Fig-
 88 ure 1B). However, post-earthquake geologic reconnaissance revealed no surface ground
 89 breaks along the proposed onland areas of EPGFZ ~~motion~~ in the epicentral region of the
 90 earthquake [Prentice *et al.*, 2010; Koehler and Mann, 2011; Rathje *et al.*, 2014]. A more
 91 recent study by Saint Fleur *et al.* [2015] proposed previously, unrecognized, 2010 coseis-
 92 mic groundbreaks along the obliquely-trending Lamentin thrust 11 km east of the epicen-
 93 tral area near the city of Port-au-Prince (Figure 2A).

94 ~~Oblique, en echelon~~ ~~En echelon~~ thrusts spacing at distances of 1-8 km along the
 95 main strike-slip fault, obliquely intersect the main strike-slip fault at angles of 30° ~~–~~
 96 45° ~~and~~. ~~These structures~~ strike northwestward away from the EPGFZ with individual
 97 oblique, fault lengths extending into the deeper basins at distances of 4-29 km (Figure 2A,
 98 Figure 3). As a result of this distinctive and regular intersecting fault geometry between
 99 these oblique thrusts and the linear ~~and continuous~~ EPGFZ, earthquake rupture initiat-
 100 ing on an oblique thrust, as seen for the Léogâne fault in 2010, is likely confined to that
 101 vicinity and may not connect with other oblique thrusts or even the EPGFZ itself [Douilly
 102 *et al.*, 2013, 2015].

103 Coseismic deformation along a large transpressional strike-slip fault, such as the
 104 EPGFZ ~~and Septentrional~~ [Calais *et al.*, 2002] in Hispaniola or the San Andreas fault
 105 zone in California [Segall and Lisowski, 1990], either is accommodated by slip and ma-
 106 jor earthquakes on the main, strike-slip plate boundary fault, or is accommodated by the
 107 oblique, *en echelon* thrusts adjacent to the main fault, or is accommodated by both sets
 108 of faults (cf. compilation of types of destructive earthquakes in transpressional settings by
 109 Hayes *et al.* [2010]). Motions on distributed, *en echelon* thrusts do not necessarily spare

110 or reduce coseismic rupture on the main strike-slip fault because the *en echelon* and main
 111 strike-slip fault remain separate fault planes, and the main strike-slip fault could continue
 112 to accumulate strain. In an extreme case, plate motions become increasingly transpres-
 113 sional as seen in the case of the EPGFZ as manifested in the obliquity of GPS vectors
 114 relative to the strike of the EPGFZ (Figure 1A, B) or in a restraining bend setting or dur-
 115 ing the plate reorganizations. In ~~this~~these settings, the *en echelon*, oblique thrusts might
 116 assume more and more plate-edge strain to the point that the plate boundary behaves more
 117 like a thrust belt and less like a strike-slip boundary.

118 These oblique and *en echelon* thrust faults in transpressional settings, including
 119 large restraining bends ~~settings~~ like Hispaniola, potentially nucleate “uncharacteristic earth-
 120 quakes” of varying recurrence intervals and sizes that are distinct from the recurrence in-
 121 tervals and sizes of the adjacent but independent strike-slip fault [Fielding *et al.*, 2013].
 122 Restraining bend areas like Hispaniola can lead to the generation and increased activities
 123 on more favorably and obliquely oriented folds and thrusts whose coseismic rupture might
 124 alternate with much longer ruptures along the adjacent strike-slip fault. The number of
 125 these *en echelon*, ~~thrust faults~~thrust faults, in the restraining bend setting, can be large at
 126 observed ~~spacing~~ of 5-10 km along strike-slip faults that may be hundreds of kilometers in
 127 total length. For this reason, the identification of oblique ~~thrusts in en echelon sets~~thrusts,
 128 especially when buried or “blind”, can be ~~challenging~~, along with assessing their role in
 129 seismogenesis within a broad plate boundary and their recurrence intervals pose a major
 130 challenge for seismic hazard assessment in areas of regional transpression like Hispaniola
 131 [Frankel *et al.*, 2011].

132 2 Objectives and methods

133 ~~The objective of this paper is to better integrate the geologic structure of the 120~~
 134 ~~km-long study area, that parallels the trace of the EPGFZ and includs the 2010 epicentral~~
 135 ~~area, using a wealth of geologie, geophysics, GPS, radar interferometry, aftershock, and~~
 136 ~~modeling studies, most of which has been colleeted since the 2010 earthquake. Our main~~
 137 ~~objective is to use these information to structurally characterize the 10-15 km wide, belt of~~
 138 ~~late Holocene, transpressional deformation that forms a laterally persistent, deformed belt~~
 139 ~~along the inland, Cul-de-Sac intermontane basin in the east and the low-relief coastal plain~~
 140 ~~along Port-au-Prince bay and the Canal du Sud to the west 1B. In particular, we focus~~
 141 ~~on the identifying a family of en echelon thrusts, whose curvilinear strikes area are very~~

142 similar to the Léogâne thrust now known to be responsible for most of the energy release
 143 and coseismic uplift during the 2010 Haiti earthquake (Figure 1B, Figure 2A).

144 **2.1 Study area**

145 This elongate, belt of transpressional deformation associated with *en echelon* thrusts
 146 occupies a topographically-low, densely populated Cul-de-Sac basin underlain by poorly
 147 consolidated clastic sedimentary rocks ranging in age from Miocene to ~~recent~~ Recent
 148 [Massoni, 1955; Mann *et al.*, 1995; Terrier *et al.*, 2014; Saint Fleur *et al.*, 2015]. In east-
 149 ernmost Haiti, this belt is overlain by the shallow (33 m deep), 138 km², brackish
 150 Lake Azuey near the border separating Haiti from the Dominican Republic [Wright *et al.*,
 151 2015; Piasecki *et al.*, 2016]. Lake Enriquillo to the east is a larger, shallow (52 m), 346
 152 km², hypersaline, sub-sealevel lake located entirely in the Dominican Republic and sepa-
 153 rated from Lake Azuey by the eastward continuation of the same transpressional belt par-
 154 allel and north of the EPGFZ in the Cul-de-Sac valley [Mann *et al.*, 1995] (Figure 1B).

155 In the western part of our study area, the more transtensional segment of the EPGFZ
 156 is overlain by the shallow, 42.8 m-deep, 14 km², freshwater Lake Miragoâne (Figure 1B). All
 157 three of these shallow, inland, lakes experience variations up to 13 meters in their sur-
 158 face elevations due to annual to decadal changes in climate and rainfall amounts including
 159 extreme rainfall associated with hurricanes [Wright *et al.*, 2015; Piasecki *et al.*, 2016; Mok-
 160 nationian *et al.*, 2017; Rico, 2017].

161 **2.2 Objectives**

162 The objective of this paper is to better integrate the geologic structure of the 120
 163 km-long study area, which parallels the trace of the EPGFZ and includes the 2010 epicentral
 164 area, using a wealth of geologic, geophysics, GPS, radar interferometry, aftershock, and
 165 modeling studies, most of which has been collected since the 2010 earthquake. Our main
 166 objective is to use these information to structurally characterize the 10-15 km-wide, belt of
 167 late Holocene, transpressional deformation that forms a laterally-persistent, deformed belt
 168 along the inland, Cul-de-Sac intermontane basin in the east and the low-relief coastal plain
 169 along Port-au-Prince bay and the Canal du Sud to the west (Figure 1B). In particular, we
 170 focus on the identifying a family of *en echelon* thrusts, whose curvilinear strikes area are
 171 very similar to the Léogâne thrust now known to be responsible for most of the energy

172 [release and coseismic uplift during the 2010 Haiti earthquake](#) [Calais *et al.*, 2010; Douilly
 173 *et al.*, 2013, 2015] ([Figure 1B](#), [Figure 2A](#)).

174 **[2.3 Survey design](#)**

175 In order to understand the geologic and structural styles of transpression within this
 176 belt, including the age relations between deformation in the north-flanking belt and the
 177 EPGFZ itself, we collected a total of 94 km of high-resolution (2-10 kHz) sonar profiles
 178 in 2014 from the 138 km², brackish Lake Azuey ([Figure 2A, B](#)) and 37 km of profiles
 179 from the 14 km², fresh-water Lake Miragoâne (Figure 1B). The EPGFZ strikes through
 180 both of the lakes, so 80% of our [grid survey lines](#) on Lake Azuey and 90% of our [grid](#)
 181 [survey lines](#) on Lake Miragoâne was dedicated to the across fault-strike, north-south pro-
 182 files([Figure 1B](#)).

183 The average speed of the boat towing the sonar was 3 knots, and we used a sonar
 184 pulse rate of 4 per second. Our 2-10 kHz sonar frequency range gives sub-bottom layer
 185 resolution of about 10 cm. These surveys were the first sonar surveys in Haitian lakes.
 186 Both lakes straddle the [possible](#) active trace of Haiti's EPGFZ and its adjacent, transpres-
 187 sional fold-thrust belt, therefore provide new constraints on the location, structural style,
 188 and timing of deformation within both structural provinces. We incorporate these lake
 189 data with previous geologic mapping, geophysical observations related to the 2010 earth-
 190 quake, and regional information on plate motions in this region (Figure 1B).

191 **3 Tectonic setting of transpressional deformation in south-central Haiti including
 192 unresolved tectonic and structural questions**

193 **3.1 Previous strike-slip deformational model vs. Haiti thrust belt deformational
 194 model**

195 There are two regional structural models, [regarding the driving force and the movement](#)
 196 [along the EPGFZ](#), to explain the present-day structure of the broad, 250 km-wide zone of
 197 transpression spanning the entire width of the island of Hispaniola.

198 **3.1.1 Strike-slip, regional structural model**

199 The first is the strike-slip-dominated model, driven by oblique motion and trans-
 200 pression between the thick and buoyant [Bahama](#)-[Bahamas](#) platform on the North Amer-

ica plate, the Caribbean plate, and the Gonâve ~~plate-microplate~~ [Mann *et al.*, 1995; Dolan *et al.*, 1998; Mann *et al.*, 2002; Calais *et al.*, 2002, 2016] (Figure 1A, B). Structures and tectonic geomorphology formed in this 250 km-wide, ~~transpressional-transpressional~~ zone include: ① The GPS studies [Calais *et al.*, 2002, 2010; Hayes *et al.*, 2010; Symithe *et al.*, 2013; Douilly *et al.*, 2013, 2015] reveal the strain partitioning along the EPGFZ and the subparallel Septentrional strike-slip fault zone (the plate boundary between North Hispaniola microplate and Hispaniola microplate along the north side of the ~~island as known from GPS studies ; 2) as Hispaniola island~~) (Figure 1A). As a result of transpression, the central Hispaniola has the highest topography, up to 3 km, in all of the northern Caribbean region~~+3)~~. The left-lateral strike-slip rupture of the EPGFZ in the 18th century inferred from historical earthquakes [Bakun *et al.*, 2012] with average left-lateral offset amounts of 1.3 – 3.3 m as expressed along offset streams of the EPGFZ [Prentice *et al.*, 2010] and by left-lateral, channel offsets of 7 – 8 m along stream channels by the Septentrional fault zone ;④ [Prentice *et al.*, 1993; Leroy *et al.*, 2015]. Saint Fleur *et al.* [2015]^s study indicates the folding and thrusting of 10 – 15 km-wide belt of Miocene to Quaternary rock adjacent to the EPGFZ~~; and 5)~~. In addition, [Mann *et al.*, 2002; Grindlay *et al.*, 2005; Kroehler *et al.*, 2011] suggest a strong, southwestward, backthrusting of the Gonâve microplate, in southern Hispaniola in Haiti and Dominican Republic to the southwest onto the Caribbean plate (Figure 1B, C). Southwestward ~~backthusting-backthrusting~~ of Hispaniola is manifested by the accretionary wedges present along the Muerto trench south of the Dominican Republic [Bien-Aimé Momplaisir, 1986; Bruña *et al.*, 2009] (Figure 1B) and along the southern margin of Haiti (South Haiti accretionary prism [Bien-Aimé Momplaisir, 1986] (Figure 1C), along with the associated, localized, negative gravity anomaly associated with plate flexure under a thrust load [Mann *et al.*, 2002; Bruña *et al.*, 2009] (Figure 1A)).

226 3.1.2 Criticisms of the strike-slip, regional structural model

227 Two criticisms have been proposed for the strike-slip model. First, Corbeau *et al.*
 228 [2016] has questioned whether the predictions of the GPS-based block models, which pre-
 229 dict significant shortening, are ~~accurate~~ that little transpression-related shortening can be
 230 observed from regional seismic profiles in the offshore area of the Gulf of Gonâve north
 231 of the southern peninsula of Haiti, or in the area of the Jamaica Passage east of Haiti.
 232 Second, Symithe and Calais [2016] have proposed that there is no geologic evidence for

233 a continuation of the EPGFZ east of latitude 72.27°W in the eastern Cul-de-Sac Valley,
 234 Lake Azuey and Lake Enriquillo in the Dominican Republic (Figure 1B). Instead, *Symithe*
 235 and *Calais* [2016] propose that large rates of north-south shortening predicted from GPS
 236 block models is taken up entirely by low-angle thrust structures in the eastern Cul-de-Sac
 237 and Enriquillo Valleys that were modeled using GPS data as part of their study.

238 **3.1.3 Trans-Haitian fold-and-thrust belt regional structural model**

239 The Trans-Haitian fold-and-thrust belt model originated with a study by *Pubellier*
 240 *et al.* [2000], who proposed a low-angle southwestward-verging fold-and-thrust belt along
 241 the southwestern edge of the central Hispaniola block. The thrust front of this feature was
 242 thought to be actively propagating from the main Trans-Haitian fold-and-thrust belt, lo-
 243 cated in the Chaîne des Matheux ~~, (Figure 1B, Figure 2A)~~, southwestward into the area
 244 of the Léogâne plain and the Cul-de-Sac basin, further more, emerging into ~~, as what we~~
 245 ~~are proposing in this paper,~~ the transpressional belt along the northern flank of the EPGFZ
 246 (Figure 2A, B). *Pubellier et al.* [2000] proposed that the EPGFZ originally formed as a
 247 left-lateral strike-slip fault, but became inactive in the late Miocene when deformation in
 248 southern Hispaniola became compressional and the Trans-Haitian fold-and-thrust belt had
 249 propagated into the southern area of the Cul-de-Sac basin and Léogâne plain, where it
 250 emerged or “daylighted” to form the *en echelon*, convergent structures (compiled on the
 251 map in Figure 2). *Pubellier et al.* [2000] also proposed that the EPGFZ was reactivated
 252 as a normal fault in the Quaternary as a result of crustal loading of the southern, foreland
 253 area by the overthrusting Trans-Haitian fold-and-thrust belt.

254 Following the 2010 earthquake and the recognition of the north-dipping blind Léogâne
 255 thrust fault, *Calais et al.* [2010] proposed that this fault is the leading edge of the Trans-
 256 Haitian fold-and-thrust belt rather than being an *en echelon* thrust genetically linked to
 257 the EGPZ, ~~as we propose in this paper based on the geologic data compiled on Figure 2A,~~
 258 **B.** In the interpretation proposed by *Calais et al.* [2010], the northward dip of the Léogâne
 259 thrust made it difficult to link its origin with the EPGFZ, whose dip had been established
 260 in this area as a vertical to high angle (> 60°), south-dipping fault plane with evidence of
 261 late Holocene, left-lateral offsets of drainages [*Prentice et al.*, 2010]. Moreover, *Symithe*
 262 and *Calais* [2016] noted that Trans-Haitian fold-and-thrust belt regional model of *Pubel-*
 263 *lier et al.* [2000] was more consistent with an increasing amount of GPS data supportive
 264 of a larger magnitude, north-south shortening in central Hispaniola than with the existence

265 of an eastward extension of the left-lateral EPGFZ into the eastern part of Haiti and the
 266 Dominican Republic (Figure 1B and Figure 2A).

267 **3.1.4 Criticisms of the Trans-Haitian fold-and-thrust belt, regional structural model**

268 First, *Mercier de Lépinay et al.* [2011] pointed out two problems with linking the
 269 origin of the Léogâne thrust to the southwestward-propagating edge of the Trans-Haitian
 270 fold-and-thrust belt: 1) the dip of the fault generating the main thrust, derived by *the*
 271 *Mercier de Lépinay et al.* [2011], was more steeply dipping (64°) than expected for a blind
 272 thrust at the leading edge of a fold-thrust belt; and 2) the orientation of the N84°E fault
 273 plane of the main shock is significantly oblique to the N120°E-oriented leading edge of
 274 the Trans-Haitian fold-and-thrust belt as proposed by *Pubellier et al.* [2000]. In this *paper*
 275 we discuss other inconsistencies with the zone of deformation north of the EPGFZ being
 276 the result of southwestward propagation of the Trans-Haitian fold-and-thrust belt.

277 **4 New observations of the Late Holocene structural style along EPGFZ in southern**
 278 **Haiti**

279 **4.1 Significance of *en echelon* thrusting and folding north and south of the**
 280 **EPGFZ**

281 The presence of a strike-slip fault at any scale is indicated by the presence of *en echelon*
 282 arrays of thrust faults, normal faults, folds, fractures, dikes, and other linear features in
 283 narrow, elongate zones [Sylvester, 1988]. On Figure 2A, we have compiled geologic infor-
 284 mation on *en echelon* folds and faults in a 10 – 15 km-wide zone of deformation along
 285 both the northern and southern flanks of the EPGFZ. Folds form as fault propagation folds
 286 along oblique thrust faults, vary from 1 to 8 km in lateral spacing; and deform Miocene
 287 and younger fine to coarse-grained, basinal, and coastal plain rocks in the belt that is 10
 288 – 15 km wide and extends parallel to the EPGFZ for 120 km (Figure 1B and Figure 2A).
 289 Folds in Neogene clastic lithologies of the Cul-de-Sac basin contrast with more continuous
 290 and longer wavelength, *en echelon* fold axes present in more massively-bedded Creta-
 291 ceous to Eocene rigid, basaltic, and carbonate lithologies exposed in the 2 km-high range
 292 south of the EPGFZ, the Massif de Selle (Figure 2B). The trend of fold axes is similar
 293 to the north and south of the EPGFZ (Figure 2B).

294 The *en echelon* distribution of complex Holocene folding and thrusting in the 10
 295 – 15 km wide zone of deformation north of the EPGFZ is also reflected in the complex
 296 pattern of 2010 coseismic and vertical deformation recorded by the interferogram from
 297 the 2010 epicentral area on the Léogâne plain west of the Cul-de-Sac basin [Hayes *et al.*,
 298 2010; Hashimoto *et al.*, 2011; Bilham and Fielding, 2013] (Figure 2A). Douilly *et al.* [2013,
 299 2015] and Kocel *et al.* [2016] use aftershocks and shallow geophysics to show that the
 300 2010 Léogâne thrust fault and sub-parallel faults are overlain by at least one kilometer
 301 of undeformed and sub-horizontal strata.

302 **4.2 Significance of curvilinear fold and thrust patterns in the transpressional belt**
 303 **north of the EPGFZ**

304 The shaded relief DEM (digital elevation model) shown in Figure 2B reveals the
 305 curvilinear, *en echelon* fold morphologies that are defined by low, bedrock hills of Neo-
 306 gene sedimentary rocks exposed on the flat-lying Cul-de-Sac basin. These curvilinear fold
 307 axes can be related directly to a broad zone of left-lateral, simple shear produced along
 308 the sub-vertical and left-lateral EPGFZ based on several, basic observations seen on Fig-
 309 ure ~~figure2B: 1) the~~ 2B. ~~The~~ most prominent folds are present along the southern edge
 310 of the Cul-de-Sac basin within 15 km of the EPGFZ; ~~in~~. In contrast, the central and
 311 northern edges of the Cul-de-Sac basin exhibit no prominent folding even directly adja-
 312 cent to the base of Eocene-Miocene carbonate rocks forming the range [Pubellier *et al.*,
 313 2000] (Figure 2A): ~~2) as typical broad zones of shearing on the thick, sedimentary rocks~~
 314 ~~as shown schematically in the inset of Figure 2B (modified from)~~, ~~the~~. The fold axes
 315 along the southern margin of the Cul-de-Sac basin are asymptotic, or gently curve into
 316 east-west parallelism with the main trace of the EPGFZ along the southern edge of the
 317 Cul-de-Sac basin; ~~3) deeper~~, as typical broad zones of shearing on the thick, sedimentary
 318 rocks (see the inset of Figure 2B; modified from Odonne and Vialon [1983]). Deeper,
 319 structural depressions form in the zone of convergent intersection between the east-west-
 320 striking EPGFZ and the northwest-striking, secondary thrusts as seen in the southern part
 321 of Lake Azuey, where the lake bends from an east-west trend adjacent to the EPGFZ to a
 322 more northwest trend in the central and northern part of the basin (Figure ~~figure2A, B~~);
 323 ~~and 4) in our sonar mapping of Lake Azuey described below, we observed late Holocene~~
 324 ~~lake sediments onlapping onto local highs of Eocene limestone of the bounding range~~

325 along the northern edge of the lake with no evidence of late Holocene faulting or folding
 326 as observed with the EPGFZ along the southern edge of the lake (Figure 2A).

327 On a more regional scale, these observations from Lake Azuey are consistent with
 328 the Canadian Superior 2D 2A, multi-channel, seismic reflection profile (shown in Figure 1C),
 329 that shows a lack of intensive deformation in the northern part of Port-au-Prince Bay, that
 330 is the offshore, largely un-faulted and folded seaward extension of the Cul-de-Sac basin.
 331 proposes that the Trans-Haitian fold-and-thrust belt exposed in the Chaine des Matheux
 332 range north extends beneath the entire Cul-de-Sac and Port-au-Prince basins (Figure 2A,
 333 B). In summary, our observations at this scale do not support the previous model by and
 334 that folds and faults of the northern range are propagating southwestward beneath the zone
 335 of *en echelon* faults and folds (Figure 2A, B).

336 **4.3 Geologic structure of the area of *en echelon* thrusts in the epicentral area on**
 337 **the Léogâne fan-delta**

338 **4.3.1 Geologic structure of the Léogâne fan area**

339 A cross sectional profile of the 2010 epicentral area related to the activation of two ;
 340 conjugate thrust faults was modified from aftershock data from Douilly *et al.* [2013, 2015]
 341 is shown in Figure 3 (Line A–A'). Both faults are buried by about 1 km of late Quater-
 342 nary sand and gravel of the Léogâne fan delta [Kocel *et al.*, 2016] and an additional 1
 343 km of Paleocene limestone. Aftershocks indicate that the main thrust event ruptured a
 344 depth range of from 4 to 17 km beneath the ground surface [Douilly *et al.*, 2013, 2015].
 345 The orientation of the Léogâne thrust based on gravity and uplift of coastal features is
 346 east-west and parallel to recent near-surface breaks of the EPGFZ mapped in the shal-
 347 low, coastal zone adjacent to the Léogâne plain [Hornbach *et al.*, 2010]. Due to its prox-
 348 imity to the EPGFZ, an east-west strike of the Léogâne thrust is predicted as this is the
 349 area where *en echelon* folds and faults curve into an asymptotic orientation relative to the
 350 main EPGFZ, as shown on Figure 2B.

351 A radar interferogram compiled on the structure map of Figure 2A revealed that the
 352 2010 earthquake elevated the smaller folds of the Léogâne fan-delta north of the EPGFZ,
 353 yet produced coseismic subsidence in the 1.4 km-high, less complexly deformed, mountain
 354 range south of the EPGFZ to the south [Hashimoto *et al.*, 2011] (Figure 2A). This para-
 355 dox can be simply explained by the northward dip of the seismogenic Léogâne fault that

356 elevated the basinal area to the north (hanging wall of the Léogâne fault) and depressed
 357 the mountainous area to the south (footwall block of the Léogâne fault (line A–A' in Fig-
 358 ure 3).

359 **4.3.2 Geologic structure of the ~~greater~~ Port-au-Prince urban area compared to the**
 360 **Léogâne epicentral area**

361 A similar pattern of deformation is observed in Port-au-Prince urban area where the
 362 central and northern edge of the Cul-de-Sac basin is almost undeformed [Massoni, 1955;
 363 Cox *et al.*, 2011; McHugh *et al.*, 2011; Saint Fleur *et al.*, 2015] (Line B-B' in Figure 3).
 364 The cross section taken from workers, who were mapping 60 years ago when the city was
 365 smaller and the geology was less obscured, shows two large thrusts, a range-bounding
 366 thrust along the southern edge of the city, and a north-dipping thrust, the Dumay thrust,
 367 that elevates a broad outcrop zone of north-dipping, Neogene sedimentary rocks on which
 368 the northern part of the city is built [Rathje *et al.*, 2014]. The 50° northeast dip of the
 369 Dumay thrust is similar to the 70° northeast dip of the Léogâne thrust to the west known
 370 from aftershocks [Douilly *et al.*, 2013, 2015], although the dip of the Dumay thrust re-
 371 verses to a southwest dip as it approaches the EPGFZ (Figure 2A, B). On the cross sec-
 372 tion B–B' in Figure 3, we have schematically indicated areas that are elevated as a result
 373 of the northward dip of the Dumay thrust and the depression of the area to the south of
 374 the EPGFZ in the highlands south of the EPGFZ. If a future earthquake occurred along
 375 the north-dipping, *en echelon* thrust faults in the Port-au-Prince are-area (Line B–B'
 376 in Figure 3) or Lake Azuey area (Line C–C' in Figure 3) a similar uplift phenomenon
 377 probably would occur where the lowlands are uplifted and the adjacent mountains subside.

378 **4.3.3 Geologic structure of the Lake Azuey area**

379 Structural cross-sections (Figure 3) from this and the previous works (Line A–A' and
 380 In the Lake Azuey area, we mapped a linear and east-west striking fault trace in deformed
 381 Holocene sediments along with its landfall (Figure 4 and Figure 5A, B). Integrated with
 382 previous land mapping of the EPGFZ [Bourgueil *et al.*, 1988; Mann *et al.*, 1995; Prentice
 383 *et al.*, 2010; Cowgill *et al.*, 2012], we interpret this linear east-west striking feature in Lake
 384 Azuey as a 5 m-wide and continuous trace of the EPGFZ which we can follow westward
 385 to the EPGFZ locality at Dumay, about half way between Lake Azuey and Port-au-Prince,
 386 which was previously described and dated as a 6 m-long, left-lateral offset of a late Holocene

387 stream channel [Cowgill *et al.*, 2012] (locates at red circle, which is labeled as Dumay
 388 in Figure 2A). The structural cross sections in this area taken from the previous studies
 389 [Massoni, 1955; Mann *et al.*, 1995; Douilly *et al.*, 2015] indicate that the high-angle EPGFZ
 390 co-exists with the adjacent thrusts that over-thrust from the south and north (Line B–B'
 391 in Figure 3) along this 120 km-long zone of deformation adjacent to the EPGFZ (3). We
 392 project this trace of the EPGFZ along a prominent fault valley at the town of Jimani that
 393 separates Lakes Azuey and Enriquillo (Figure 2A and Figure 4). Sonar profiles (Figure 5A,
 394 B) show that the oblique thrust faults share a similar orientation with other north-dipping
 395 thrusts along the northern edge of most recent rupture of the EPGFZ is covered by about
 396 0.7 m of Holocene sediment, suggesting that there has been late Holocene activity of the
 397 EPGFZ along the southern edge of the EPGFZ. All three of these oblique thrust faults
 398 shown on the cross sections deform rocks as young as Pliocene and Quaternary lake.

399 In our sonar survey of Lake Azuey From sonar data, we observed late Holocene lake
 400 sediments onlapping onto local highs of Eocene limestone of the bounding range along the
 401 northern edge of the EPGFZ (Figure 5). The sonar from southern Lake Azuey suggests
 402 that the most prominent folds present adjacent to the EPGFZ become less prominent in
 403 the central and northern parts of the lake (Figure 2B). These southern folds and thrusts
 404 imaged in Lake Azuey define the transpressive belt along the EPGFZ observed in onshore
 405 areas to the west. On the cross section C–C' in Figure 35C, we have schematically indi-
 406 cated areas that are elevated as a result of the northward dip of the Jimani thrust and the
 407 depression of the area to the south of the EPGFZ in the highlands south.

408 The structural cross-section (Figure 5C) of the Lake Azuey area and the previous
 409 works [Massoni, 1955; Bourgueil *et al.*, 1988; Cox *et al.*, 2011; Douilly *et al.*, 2015] (Line
 410 A–A' and B–B' in Figure 3) along this 120 km-long zone of deformation adjacent to the
 411 EPGFZ show that the oblique thrust faults share a similar orientation with other northeast-dipping
 412 thrusts along the northern edge of the EPGFZ. All three of these oblique thrust faults (the
 413 Léogâne thrust in Line A–A', the Dumay thrust in Line B–B', and the Jimani thrust in
 414 Figure 5C) shown on the cross sections deform rocks as young as Pliocene and Quaternary
 415 [Saint Fleur *et al.*, 2015].

416 On a more regional scale, these observations from Lake Azuey are consistent with
 417 the multi-channel seismic reflection profile (named as Canadian Superior 2D and shown
 418 in Figure 1C), that shows a lack of intensive deformation in the part of Port-au-Prince

419 Bay, that is the offshore, largely un-faulted and folded seaward extension of the Cul-de-Sac
 420 basin [McHugh *et al.*, 2011]. Pubellier *et al.* [2000] proposes that the Trans-Haitian fold-and-thrust
 421 belt exposed in the Chaine des Matheux range north extends beneath the entire Cul-de-Sac
 422 and Port-au-Prince basins (Figure 2A, B). In summary, our observations at this scale do
 423 not support the previous model by Pubellier *et al.* [2000] and Calais *et al.* [2010] that
 424 folds and faults of the northern range are propagating southwestward beneath the zone
 425 of *en echelon* faults and folds (Figure 2A, B).

426 **4.4 Subsurface stratigraphy of Lake Azuey and Lake Enriquillo and paleoseis-
 427 mic estimates of the relative timing of recent earthquakes on the EPGFZ and
 428 secondary, *en echelon* thrust faults**

429 Our objective is to determine the relative age of the EPGFZ and its adjacent zone
 430 of fold-and-thrust deformation using the sonar profiles from Lakes Azuey and Enriquillo
 431 (Figure 6A). Both previous coring The previous coring, both in Lake Enriquillo [Rios *et al.*,
 432 2013], which was tied to the onshore stratigraphic studies [Taylor *et al.*, 1985; Rios *et al.*,
 433 2013], and in Lake Miragoâne [Higuera-Gundy *et al.*, 1999], have established the late
 434 Holocene sedimentary history to include the upper 5 and 7 meters of both lakes, respec-
 435 tively.

436 In Lake Enriquillo, a sonar survey similar to ours was conducted in 2013 [Rios
 437 *et al.*, 2013]. Mapping in both lakes revealed the presence of the east-west strands of
 438 the EPGFZ that are collinear with onshore scarps both east and west of Lake Azuey (Fig-
 439 ure 2, Figure 6, and Figure 4) and east and west of Lake Enriquillo [Mann *et al.*, 1995;
 440 Rios *et al.*, 2013]. These east-west fault strands abruptly truncate the trends of folds in the
 441 ranges south of the lake (Figure 4).

442 In Lake Enriquillo, a sonar survey similar to ours was conducted in 2013. The
 443 sonar events, which are interpreted as stratigraphic features, from Lake Azuey and Lake
 444 Enriquillo (Line B1 and Line L19 correlate convincingly (Figure 6B). Given the small
 445 distance separating the two lakes (about 4 km); the similarity of the stratigraphic pro-
 446 files; and the same amount of sediment above the EPGFZ; it is reasonable to suggest that
 447 Lake Azuey and Lake Enriquillo share the same sedimentation history as well as the same
 448 structural style and seismicity related to the EPGFZ and its oblique, thrust faults.

449 The EPGFZ in both Lake Enriquillo and Lake Azuey is buried by 0.7 m of sedi-
 450 ments. According to coring studies in the Dominican Republic [Taylor *et al.*, 1985; Rios
 451 *et al.*, 2013], the 5.2 m thickness of the latest lake stage (2 ka BP to present) gives a re-
 452 cent Holocene average sedimentation rate of 2.6 mm/yr (Figure 6B). Using the average
 453 sediment rate, the most recent rupture of the EPGFZ would be dated some 270 years ago.
 454 Given the historical earthquake records [Bakun *et al.*, 2012], we suggest that the most re-
 455 cent rupture of the EPGFZ is correspond to the historical events of October or November
 456 of 1751, and the deformed sediments in Lake Azuey are in Holocene age.

457 **4.5 Mapping of the EPGFZ trace from sonar data in deformed lake sediments of 458 Lake Azuey, Haiti**

459 In the Lake Azuey area (Figure 2A), we mapped a linear and east-west striking fault
 460 trace in deformed Holocene sediments along with its landfall (Figure 6A, B and Figure 4).
 461 Integrated with previous land mapping of the EPGFZ, we interpret this linear east-west
 462 striking feature in Lake Azuey as a 5 m-wide and continuous trace of the EPGFZ which
 463 we can follow eastward to the EPGFZ locality at Dumay, about half way between Lake
 464 Azuey and Port-au-Prince, which was previously described and dated as a 6 m-long, left-lateral
 465 offset of a late Holocene stream channel (shown in Figure 2A).

466 The structural cross sections in this area taken from the previous studies indicate
 467 that the high-angle EPGFZ co-exists with the adjacent thrusts that over-thrust from the
 468 south and north (Line B-B' in Figure 3). Sonar profiles from the southernmost area of
 469 Lake Azuey (Figure 5) show that the most recent rupture of the EPGFZ is covered by
 470 about 0.7 m of Holocene sediment, suggesting that there has been no recent activity of
 471 the EPGFZ. We project this trace of the EPGFZ along a prominent fault valley at the town
 472 of Jimani that separates Lakes Azuey and Enriquillo (Figure 2A and Figure 4).

473 **4.5 Easternmost extent of the EPGFZ trace in Lake Enriquillo, Dominican Re- 474 public**

475 Based on both of our lake surveys combined with a previous survey of Lake En-
 476 riquillo in the Dominican Republic [Rios *et al.*, 2013], and the previous geologic mapping
 477 of the basinal and topographic corridor of the Cul-de-Sac basin in Haiti and the Enriquillo
 478 basin in the Dominican Republic [Mann *et al.*, 1995; Mann, 1999], a first-order question

479 we pose is whether the EPGFZ extends as a continuous, strike-slip fault along the 120
 480 km-long zone of deformation of Miocene and younger clastic rocks present between the
 481 two lakes ([Figure 1B](#) and [Figure 6A](#)). The previous studies [*Saint Fleur et al.*, 2015;
 482 *Symithe and Calais*, 2016] have proposed that the EPGFZ terminates as a strike-slip fea-
 483 ture in the area south of Port-au-Prince. These studies further ~~propose~~have proposed that
 484 transpressional plate motion in the eastern Cul-de-Sac basin and the Enriquillo Valley in
 485 the Dominican Republic ([Figure 1B](#) and [Figure 6A](#)) is entirely accommodated along the
 486 low-angle oblique-thrust structures that overthrust the southern edges of Lake Azuey and
 487 Lake Enriquillo([Figure 1B](#) and [Figure 6A](#)).

488 A previous study of Lake Enriquillo by *Rios et al.* [2013] identified the break along
 489 the northeastern edge of Cabritos Island in Lake Enriquillo, which aligns exactly with the
 490 large east-western lineament extending eastward from our map area in Lake Azuey (Fig-
 491 ure 6A). The sonar results from both lakes show that the EPGFZ extends to at least to the
 492 eastern tip of Cabritos Island in the center of Lake Enriquillo, Dominican Republic (Fig-
 493 ure 6A). This survey revealed a fault penetrating the youngest sediment layer of Holocene
 494 age which is consistent with recent activity on this segment of the EPGFZ (Figure 5A, B).
 495 ~~Therefor~~Therefore, we conclude that this linear, late Holocene strike-slip fault extends at
 496 55 km (at least) to the eastern edge of Lake Enriquillo, where the ~~recently documented~~
 497 previously documented [*Mann et al.*, 1995] uplift of the Holocene reef fringes Lake En-
 498 riquillo.

499 5 Active tectonics of the area west of the 2010 epicentral zone in the western study 500 area: [Léogâne plain, Miragoâne basin, and their adjacent offshore area](#)

501 5.1 [The Trois Baies thrust fault, Canal du Sud, as a](#) termination structure for 502 the 2010 earthquake

503 The 2010 aftershock zone at the western and central part of our study area (Fig-
 504 ure 7A) reflects the rupture along the northwest-striking, 20 km-long, submarine, Trois
 505 Baies thrust fault that forms the western extension of the 10 – 15 km-wide, transpressional
 506 zone north of the EPGFZ. As the Trois Baies fault is submarine, InSAR cannot be used
 507 to assess its 2010 coseismic similarity with folding and thrusting along the Léogâne thrust
 508 that affected the onshore, Léogâne plain (Figure [7A](#)).

509 However, the same basic structural elements of the Léogâne plain are also observed
 510 for the Trois Baies thrust fault, which include the short distance (1 km) to the EPGFZ and
 511 its steep (45°) but opposite (southwest) dip of the Trois Baies thrust fault (Figure 7A).
 512 One of the most intense zones of coseismic, aftershock, and coastal uplift separates the
 513 oppositely-dipping Léogâne and Trois Baies faults, and may represent complex defor-
 514 mation at a transfer zone between the two faults (Figure 7A). The aftershock study of
 515 the Trois Baies fault [Symithe and Calais, 2016] shows that ~~it~~its geological structure of
 516 thrust faulting and spacial oblique relationship with the main EPGFZ is comparable to
 517 the cross sections of the eastern area in Figure 3. ~~The~~Also, in the map view, the overall
 518 structure of this western part of the study area mirrors the same ~~geometry of geometrical~~
 519 relationship between the oblique thrusts (such as the Trois Baies thrust fault) and the main
 520 EPGFZ described at the eastern part of the study area (Figure 2).

521 5.2 Structure of the Miragoâne pull-apart basin

522 In the onshore part of the western study area, Lake Miragoâne was interpreted as a
 523 14 km² pull-part basin developed as a left-stepping, releasing bend on the EPGFZ paired
 524 with the adjacent Tapion du Petit Goâve restraining bend 12 km to the east (Figure 7)
 525 [Cowgill *et al.*, 2012]. Bathymetry from our sonar data shows the maximum water depth
 526 of Lake Miragoâne is 42.8 m (Figure 7B), which makes this ~~actively faulted~~ lake the deepest
 527 [Higuera-Gundy *et al.*, 1999] in the Caribbean region. The 30 m of recognizable stratig-
 528 raphy (Figure 8A, ~~B~~B and C) from the sonar survey in Lake Miragoâne reveals a series
 529 of deformational features including major east-west normal faults, minor thrust faults at
 530 ~~deep depth~~ (some 20 m), and active folds at the lake bottom (Figure 8). The upper 7 m
 531 meters of the lake ~~sediment was sediments were~~ cored and dated ~~as at~~ 10 ka at the bot-
 532 tom of the core ~~. Extrapolating the~~ [Higuera-Gundy *et al.*, 1999]. By applying the average
 533 sedimentary rate from the core data to the whole chirp sonar trace, we can extrapolate
 534 the sedimentation rate to the observed thickness of 30 m in the lake ~~allows and estimate~~
 535 a minimum of ~~33 ka to be calculated~~ 43 ka for the age of the pull-apart basin on the
 536 EPGFZ. Core measurements of the E/P (evaporation and precipitation ratio from the $\delta^{18}\text{O}$
 537 of ostracod shells in the core sample) were undertaken [Higuera-Gundy *et al.*, 1999] in
 538 the center of Lake Miragoâne (Figure 9B). The core reveals ~~that~~ the uppermost part of
 539 the ~~sediment is Holocene and sediments are Holocene to~~ the latest Pleistocene lacustrine

540 ([Figure in age](#) ([Figure](#) 9A)). Pollen data from the core indicate alternating dry and wet envi-
 541 ronments.

542 5.3 Ages and sedimentary cycles of the Miragoâne pull-apart basin

543 ~~Comparing the core data with the sonar data, we can see the sediment layers from~~
 544 ~~drier climates (higher E/P) correlate with stronger acoustic reflectivity and vice versa~~
 545 ~~(Figure 9A).~~ We applied a low-pass filter on the pollen log data and found a strong cor-
 546 relation between the pollen and sonar data (red curve in Figure 9B). To further investi-
 547 gate this interesting correlation between the geochemical and geophysical data, we use
 548 the filtered E/P log, considered as pseudo-acoustic impedance log, to generate a synthetic
 549 sonar response (Figure 9B). The correlation is compelling which suggests that the deposi-
 550 tional environment influences the acoustic properties of the sediments and sonar response
 551 may be a partial proxy for climatic processes. [In another words, the sediment layers from](#)
 552 [drier climates \(higher E/P\) have stronger acoustic reflectivity and vice versa. The core](#)
 553 [was acquired in the center of the lake. Combining the correlation between the pollen log](#)
 554 [and the acoustic reflections from the chirp sonar data, we can extend the sedimentary](#)
 555 [history of the upper 7 meters from the log data to the entire sonar data set. In the sonar](#)
 556 [profile, we find the most recent rupture in the lake is buried by about 0.5 meter sediment](#)
 557 [\(Figure 8B, C\). The core dating result from Higuera-Gundy et al. \[1999\] suggests the age](#)
 558 [of these rupture is about 300 years old. The historical document record \[Bakun et al.,](#)
 559 [2012\] indicates a historical earthquake happened in this area in 1770.](#) Considering the
 560 historical document record [Bakun et al., 2012], the dating of the core ~~and~~ [and the](#) sonar
 561 interpretation in Lake Miragoâne suggest that the most recent rupture in this lake is likely
 562 related to ~~a~~ [the](#) historic earthquake in 1770 [Bakun et al., 2012].

563 6 Discussion

564 6.1 Proposed 3D structural model for the 10 – 15 km-wide belt of transpressional 565 deformation along the northern edge of the EPGFZ

566 In summary, our lake studies, along with previous work, favor a model of a 10 –
 567 15 km-wide transpressional zone that deforms thick, loosely-consolidated, Miocene to
 568 recent clastic rocks in coastal, marine, and lake settings as ~~shown in three dimensions~~
 569 ([Figure illustrated in three-dimensional block diagram](#) ([Figure](#) 10)). Moving from Lake

570 Azuey in the east to Lake Miragoâne in the west, the block diagram illustrates along-strike
 571 changes observed in the dips of the thrust faults and obliquely orientation to the EPGFZ.
 572 Fold axes north of the EPGFZ range from 3 to 20 km in length, and are sigmoidally re-
 573 lated to the EPGFZ in map view (Figure 2A, B). Dip direction and amounts on these
 574 thrust faults vary from north-dipping at 21° on the Jimani fault (**C–C'** in Figure 3, Fig-
 575 ure 5C and Figure 10), south-dipping on the Lamentine fault [Saint Fleur *et al.*, 2015] at
 576 40°, north-dipping at 70° on the Léogâne fault active during the 2010 earthquake (A–A' in
 577 Figure 3, Figure 10), and south-dipping on the Trois Baies fault at 45° (Figure 10).

578 South of the EPGFZ, transpressional folding in more rigid Cretaceous basalts and
 579 overlying Eocene limestone have ~~wavelengths ranging broader wavelengths~~ from
 580 1 to 8 km ~~and a weak seismogenic deformation. On the other hand,~~ InSAR images of
 581 the 2010 earthquake indicate smaller folds and more seismogenic deformation in the 10
 582 – 15 km belt north of the EPGFZ~~as opposed to the broader folding and less seismogenic~~
 583 ~~deformation south of the EPGFZ~~. This contrast is likely related to rock type with poorly
 584 consolidated sedimentary rocks up to several kilometers north of the EPGFZ and more
 585 consolidated carbonate rocks and basalts exposed in the highlands south of the EPGFZ
 586 [Mann *et al.*, 1991] (Figure 2).

587 We propose that the folds north of the EPGFZ formed originally as conjugate thrust
 588 faults, reflecting the northeast to southwest convergence indicated by GPS vectors and
 589 highly transpressional character of the EPGFZ [Calais *et al.*, 2010]. Conjugate thrust faults
 590 are common in thick, clastic sedimentary basins undergoing active, sub-horizontal short-
 591 ening [Sibson, 2012], as documented in the M_w 7.6 Chi-Chi Taiwan earthquake in 1999
 592 [Chen *et al.*, 2002] or the M_w 7.1 Kumamoto Japan earthquake in 2016 [Lin and Chiba,
 593 2017]. Aftershocks north of the EPGFZ reflect the most recent phase of NE-SW shorten-
 594 ing on the 70° dipping reverse fault planes [Nettles and Hjörleifsdóttir, 2010], along the
 595 deeply buried Léogâne thrust fault, as shown in the cross-section of A–A' in Figure 3.

596 Our results, including the eastward extension of the EPGFZ into Dominican Republic,
 597 support the “thick-skinned” strike-slip model for the deformation of Hispaniola region
 598 as opposed to the southwestward propagation of the Trans-Haitian fold-and-thrust belt
 599 proposed by .

600 **6.2 Analogy between the 2010 coseismic transpressional deformation in Haiti and**
 601 **the 1989 Loma Prieta earthquake in northern California**

602 **6.3 Is the 2010 coseismic transpressional deformation in Haiti analogous to the**
 603 **1989 Loma Prieta earthquake in northern California?**

604 A similar pattern of transpression in a restraining bend setting to Haiti has been
 605 described for 1989 M_w 6.9 Loma Prieta earthquake [Marshall *et al.*, 1991] (Figure 11).
 606 These aftershocks define a conjugate pair of reverse faults with the dominant motion on
 607 the north-dipping fault plane.

608 Features compiled on the map from various sources include: 1) The selected GPS
 609 vectors from relative to a fixed North America plate showing [UNAVCO (*University Nav-*
 610 *star Consortium*), 2009] indicate the transpressional setting in a gentle restraining bend set-
 611 ting; 2) inset map with cross-section of . In the inset map of Figure 11, the 1989 hypocen-
 612 tral area showing the main shock (yellow star) and related aftershocks (red dots) along the
 613 southwest-dipping San Andreas and Sargent faults from ; 3) documentation of the [Mar-
 614 shall *et al.*, 1991] shows the steep (~ 61°) dip of oblique-reverse faults of the collective
 615 Sargent and San Andreas faults by ; 4) Also, the 1989 coseismic elevation change with
 616 uplift of uplifted 0.55 meters on the southwestern hanging wall of the San Andreas and
 617 Sargent faults, and subsidence of subsided 0.1 meters on the northeastern footwall block
 618 ; and 5) [Marshall *et al.*, 1991]. The thrusting was blind with the M_w 7.1 earthquake not
 619 being accompanied by coseismic, ground breaks—surface breaks. These aftershocks define
 620 a conjugate pair of reverse faults with the dominant motion on the south-dipping fault
 621 plane.

622 As in the 2010 M_w 7.0 Haiti earthquake, a secondary, blind thrust fault [Olson,
 623 1990] beneath the surface trace of the Sargent fault that, and oblique to the main San An-
 624 dreas strike-slip fault (shown in inset map of Figure 11), played a major role in the 1989
 625 fault rupture and resulting pattern of regional uplift show shown in red color to the south-
 626 west and regional subsidence shown in green-blue color to the northeast (Figure 11).

627 While the oblique thrust planes form smaller fault segments ranging in length from
 628 3 to 11 km (Figure figure22A), the 2010 earthquake demonstrates that oblique thrusts
 629 like the Léogâne fault are capable of producing a M_w 7.0 earthquake with devastating re-
 630 sults, especially when coupled with inadequate construction practices [Symithe and Calais,

631 2016]. Paleoseismic estimates of the age of the most recent deformation of Lake Azuey,
 632 eastern Haiti, suggests that the latest activity of the EPGFZ in this area was in 1751 [Prentice
 633 et al., 2010; Bakun et al., 2012]. Similar analysis indicates that the latest earthquake
 634 event in the Lake Miragoâne area, western Haiti, was in 1770 [Bakun et al., 2012]. This ~~suggests~~
 635 ~~the~~, ~~agreeing the previous study by~~ Bakun et al. [2012], ~~suggest the~~ earthquake recurrence
 636 cycle along the EPGFZ is about 250 years. Therefore, in this transpressional setting, the
 637 earthquake cycle may consist of an interplay between ruptures on the EPGFZ and ruptures
 638 on the oblique thrusts and related folds.

639 The 2010 M_w 7.0 earthquake released part of the stress of the region, but as the
 640 oblique thrusts may not be directly linked to the EPGFZ, it is possible that stresses on the
 641 EPGFZ have continued to accumulate since the 18th century [Prentice et al., 2010]. Inte-
 642 grated paleoseismic study of the EPGFZ with the commonly buried oblique thrust faults,
 643 using geophysical and geologic methods, can help to inform the critical social issue of
 644 how future earthquakes will be partitioned between the larger EPGFZ and other more ob-
 645 scure, oblique faults

646 7 Conclusions

647 The main ~~conclusion~~ conclusions of the study are as follows:

648 1. ~~The devastating, 2010 Haiti earthquake (M_w 7.0) was caused by rupture of the~~
 649 ~~Léogâne blind, thrust fault located 5 km north of the main, Caribbean-Gonâve plate boundary:~~
 650 ~~a 1200 km-long, left-lateral, Enriquillo-Plantain Garden fault zone (EPGFZ). Unexpectedly,~~
 651 ~~the EPGFZ remained largely quiescent or slightly reactivated during the 2010 earthquake,~~
 652 ~~although the EPGFZ formed a line of inflection between a coseismically uplifted lowland~~
 653 ~~north of the EPGFZ and a subsided area in the highlands south of the fault.~~

654 2. ~~Here, we use high-resolution~~ High-resolution sonar data from two Haitian lakes
 655 that straddle the EPGFZ and its northern flank ~~to demonstrate~~ demonstrates the presence
 656 of a 10 – 15 km-wide, 120 km-long, late Holocene, fold-and-thrust belt, which is deform-
 657 ing both the clastic lowland basins along the northern edge of the EPGFZ and the steep
 658 topographic highlands to the south.

659 3. ~~2.~~ In the eastern part of the study area, sonar results from Lake Azuey show
 660 that the EPGFZ is more deeply buried and less active than the adjacent, newly discov-
 661 ered, northwest-striking, northeast-dipping Jimani thrust fault. This structural relation-

662 ship between the two faults is identical to the 2010 epicentral area 70 km to the west: the
 663 2010 seismogenic, Léogâne blind thrust fault is northwest-to-east-striking, and the quies-
 664 cent fault to the south during the 2010 earthquake is the east-west-striking, sub-vertical
 665 EPGFZ.

666 **4–3.** The geographic distribution of 2010 aftershocks revealed that the seismogenic
 667 motions of the Léogâne thrust fault and smaller motions on the EPGFZ terminated on a
 668 similar northwest-striking fault: the submarine Trois Bains thrust fault. In the western-
 669 most part of the study area, sonar results from Lake Mirogoâne show two overlapping and
 670 active strands of the EPGFZ, and was instead diverted onto the Trois Bains thrust fault.

671 **5–4.** Our survey confirmed the pull-apart origin of Lake Mirogoâne and the lack
 672 of historical deformation on this western segment of the EPGFZ during the 2010 M_w 7.0
 673 earthquake. Integration of the geologic data across the study area show an alternation in
 674 dip along nine northwest-striking, thrust faults at spacing of 5 to 40 km.

675 **6–5.** We interpret this zone of late Holocene deformation in clastic basins north of
 676 the EPGFZ as the accommodation of transpressional strain supported by highly-oblique
 677 GPS vectors across the study area. In this transpressional zone, coseismic deformation
 678 alternates at recurrence intervals of centuries between oblique shortening structures, such
 679 as Léogâne thrusts, Jimani thrusts, and Trois Bains thrusts, and strike-slip ruptures along
 680 the narrow and well defined main trace of the EPGFZ.

681 **6. Our results, including the eastward extension of the EPGFZ into Dominican Republic,**
 682 **support the “thick-skinned” strike-slip model for the deformation of Hispaniola region**
 683 **as opposed to the southwestward propagation of the Trans-Haitian fold-and-thrust belt**
 684 **proposed by Pubellier et al. [2000].**

685 Acknowledgments

686 We would like to thank the Society of Exploration Geophysicists’ Geoscientists Without
 687 Borders program for supporting this project along with our earlier shallow-geophysical
 688 imaging of the epicentral region on the Léogâne fan [Kocel et al., 2016]. We also ex-
 689 press our appreciation to Alex von Lignau (Haiti Department of Finance), Alfredo Lo
 690 Cicero (Oxfam Italia in Haiti) for financial and logistical support on Lake Azuey. Lud-
 691 ner Remarais, and Jean Robert Altidor of the Haiti Bureau of Mines and Energy for their
 692 assistance with fieldwork, permissions, and importation of equipment. Eric Fielding of

693 JPL/Caltech for kindly providing the INSAR imagery. Roby Douilly of Purdue University
694 for generously providing location information for aftershock data. We are grateful to Al-
695 lied Geophysical Laboratories (AGL) and Will Sager at University of Houston for assisting
696 with equipment and fieldwork preparation.

697 **References**

- 698 Bakun, W. H., C. H. Flores, and S. Uri (2012), Significant earthquakes on the Enriquillo
 699 fault system, Hispaniola, 1500–2010: Implications for seismic hazard, *Bulletin of the*
 700 *Seismological Society of America*, 102(1), 18–30.
- 701 Benford, B., C. DeMets, and E. Calais (2012), GPS estimates of microplate motions,
 702 northern Caribbean: evidence for a Hispaniola microplate and implications for earth-
 703 quake hazard, *Geophysical Journal International*, 191(2), 481–490.
- 704 Bien-Aimé Momplaisir, R. (1986), Contribution à l'étude géologique de la partie orientale
 705 du Massif de la Hotte (Presqu'île du Sud d'Haïti): Synthèse structurale des marges de
 706 la presqu'île à partir de données sismiques, *PhD thesis*, p. 210.
- 707 Bilham, R. (2010), Lessons from the Haiti earthquake, *Nature*, 463(7283), 878–879.
- 708 Bilham, R., and E. Fielding (2013), Remote sensing and the search for surface rupture,
 709 haiti 2010, *Natural hazards*, 68(1), 213–217.
- 710 Bourgueil, B., P. Andreieff, J. Lasnier, R. Gonnard, J. Le Metour, and J.-P. Rancon (1988),
 711 Synthèse géologique de la République d'Haïti, in *Technical report, Bureau des Mines et*
 712 *de l'Energie*, Haiti Port-au-Prince.
- 713 Bruña, J. G., U. S. Ten Brink, A. Carbó-Gorosabel, A. Muñoz-Martín, and M. G. Balles-
 714 teros (2009), Morphotectonics of the central Muertos thrust belt and Muertos Trough
 715 (northeastern Caribbean), *Marine geology*, 263(1), 7–33.
- 716 Calais, E., Y. Mazabraud, B. Mercier de Lépinay, P. Mann, G. Mattioli, and P. Jansma
 717 (2002), Strain partitioning and fault slip rates in the northeastern Caribbean from GPS
 718 measurements, *Geophysical Research Letters*, 29(18).
- 719 Calais, E., A. Freed, G. Mattioli, F. Amelung, S. Jónsson, P. Jansma, S.-H. Hong,
 720 T. Dixon, C. Prépetit, and R. Momplaisir (2010), Transpressional rupture of an un-
 721 mapped fault during the 2010 Haiti earthquake, *Nature Geoscience*, 3(11), 794–799.
- 722 Calais, É., S. Symithe, B. M. de Lépinay, and C. Prépetit (2016), Plate boundary segmen-
 723 tation in the northeastern Caribbean from geodetic measurements and Neogene geologi-
 724 cal observations, *Comptes Rendus Geoscience*, 348(1), 42–51.
- 725 Chen, K.-C., B.-S. Huang, J.-H. Wang, and H.-Y. Yen (2002), Conjugate thrust faulting
 726 associated with the 1999 Chi-Chi, Taiwan, earthquake sequence, *Geophysical Research*
 727 *Letters*, 29(8).

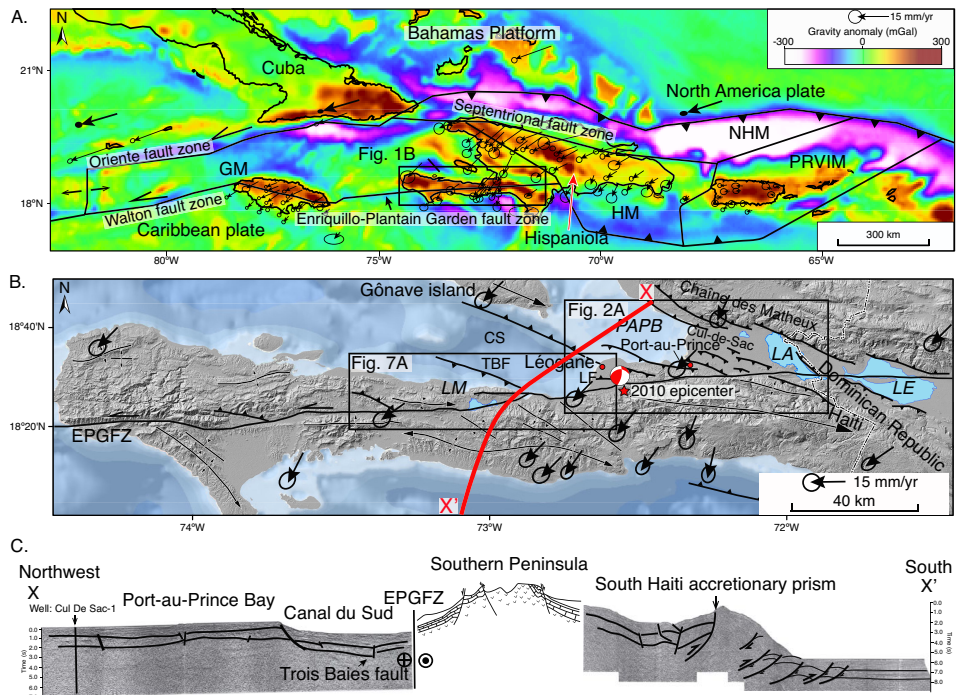
- 728 Corbeau, J., F. Rolandone, S. Leroy, B. Meyer, B. Mercier de Lépinay, N. Ellouz-
729 Zimmermann, and R. Momplaisir (2016), How transpressive is the northern Caribbean
730 plate boundary?, *Tectonics*, 35(4), 1032–1046.
- 731 Cowgill, E., T. S. Bernardin, M. E. Oskin, C. Bowles, M. B. Yıldız, O. Kreylos, A. J.
732 Elliott, S. Bishop, R. D. Gold, A. Morelan, et al. (2012), Interactive terrain visualization
733 enables virtual field work during rapid scientific response to the 2010 Haiti earthquake,
734 *Geosphere*, 8(4), 787–804.
- 735 Cox, B. R., J. Bachhuber, E. Rathje, C. M. Wood, R. Dulberg, A. Kottke, R. A. Green,
736 and S. M. Olson (2011), Shear wave velocity-and geology-based seismic microzonation
737 of Port-au-Prince, Haiti, *Earthquake Spectra*, 27(S1), S67–S92.
- 738 Dolan, J. F., H. T. Mullins, and D. J. Wald (1998), Active tectonics of the north-central
739 Caribbean: Oblique collision, strain partitioning, and opposing subducted slabs, *SPE-
740 CIAL PAPERS-GEOLOGICAL SOCIETY OF AMERICA*, pp. 1–62.
- 741 Douilly, R., J. S. Haase, W. L. Ellsworth, M.-P. Bouin, E. Calais, S. J. Symithe, J. G.
742 Armbruster, B. M. de Lépinay, A. Deschamps, S.-L. Mildor, et al. (2013), Crustal struc-
743 ture and fault geometry of the 2010 Haiti earthquake from temporary seismometer de-
744 ployments, *Bulletin of the Seismological Society of America*, 103(4), 2305–2325.
- 745 Douilly, R., H. Aochi, E. Calais, and A. Freed (2015), Three-dimensional dynamic rupture
746 simulations across interacting faults: The mw7. 0, 2010, haiti earthquake, *Journal of
747 Geophysical Research: Solid Earth*, 120(2), 1108–1128.
- 748 Fielding, E. J., A. Sladen, Z. Li, J.-P. Avouac, R. Bürgmann, and I. Ryder (2013), Kine-
749 matic fault slip evolution source models of the 2008 M7.9 Wenchuan earthquake in
750 China from SAR interferometry, GPS and teleseismic analysis and implications for
751 Longmen Shan tectonics, *Geophysical Journal International*, 194(2), 1138–1166, doi:
752 10.1093/gji/ggt155.
- 753 Frankel, A., S. Harmsen, C. Mueller, E. Calais, and J. Haase (2011), Seismic hazard maps
754 for Haiti, *Earthquake Spectra*, 27(S1), S23–S41.
- 755 Grindlay, N. R., M. Hearne, and P. Mann (2005), High risk of tsunami in the northern
756 Caribbean, *Eos, Transactions American Geophysical Union*, 86(12), 121–126.
- 757 Hashimoto, M., Y. Fukushima, and Y. Fukahata (2011), Fan-delta uplift and mountain sub-
758 sidence during the haiti 2010 earthquake, *Nature Geoscience*, 4(4), 255–259.
- 759 Hayes, G., R. Briggs, A. Sladen, E. Fielding, C. Prentice, K. Hudnut, P. Mann, F. Taylor,
760 A. Crone, R. Gold, et al. (2010), Complex rupture during the 12 January 2010 Haiti

- 761 earthquake, *Nature Geoscience*, 3(11), 800–805.
- 762 Higuera-Gundy, A., M. Brenner, D. A. Hodell, J. H. Curtis, B. W. Leyden, and M. W.
763 Binford (1999), A 10,300 14 C yr record of climate and vegetation change from Haiti,
764 *Quaternary Research*, 52(2), 159–170.
- 765 Hornbach, M. J., N. Braudy, R. W. Briggs, M.-H. Cormier, M. B. Davis, J. B. Diebold,
766 N. Dieudonne, R. Douilly, C. Frohlich, S. P. Gulick, et al. (2010), High tsunami fre-
767 quency as a result of combined strike-slip faulting and coastal landslides, *Nature Geo-
768 science*, 3(11), 783–788.
- 769 Kocel, E., R. R. Stewart, P. Mann, and L. Chang (2016), Near-surface geophysical investi-
770 gation of the 2010 Haiti earthquake epicentral area: Léogâne, Haiti, *Interpretation*, 4(1),
771 T49–T61.
- 772 Koehler, R., and P. Mann (2011), Field observations from the January 12, 2010, Haiti
773 earthquake: Implications for seismic hazards and future post-earthquake reconnaissance
774 investigations in Alaska, *Report of Investigations*, 2, 24.
- 775 Kroehler, M. E., P. Mann, A. Escalona, G. Christeson, et al. (2011), Late Cretaceous-
776 Miocene diachronous onset of back thrusting along the South Caribbean deformed belt
777 and its importance for understanding processes of arc collision and crustal growth, *Tec-
778 tonics*, 30(6).
- 779 Leroy, S., N. Ellouz-Zimmermann, J. Corbeau, F. Rolandone, B. M. Lépinay, B. Meyer,
780 R. Momplaisir, J.-L. Granja Bruña, A. Battani, C. Baurion, et al. (2015), Segmentation
781 and kinematics of the North America-Caribbean plate boundary offshore Hispaniola,
782 *Terra Nova*, 27(6), 467–478.
- 783 Lin, A., and T. Chiba (2017), Coseismic conjugate faulting structures produced by the
784 2016 m w 7.1 kumamoto earthquake, japan, *Journal of Structural Geology*, 99, 20–30.
- 785 Mann, P. (1999), Caribbean sedimentary basins: Classification and tectonic setting from
786 Jurassic to present, *Sedimentary Basins of the World*, 4, 3–31.
- 787 Mann, P., G. Draper, J. F. Lewis, et al. (1991), An overview of the geologic and tectonic
788 development of hispaniola, *Geologic and tectonic development of the North America-
789 Caribbean plate boundary in Hispaniola. Geological Society of America Special Paper*,
790 262, 1–28.
- 791 Mann, P., F. Taylor, R. L. Edwards, and T.-L. Ku (1995), Actively evolving microplate
792 formation by oblique collision and sideways motion along strike-slip faults: An example
793 from the northeastern Caribbean plate margin, *Tectonophysics*, 246(1), 1–69.

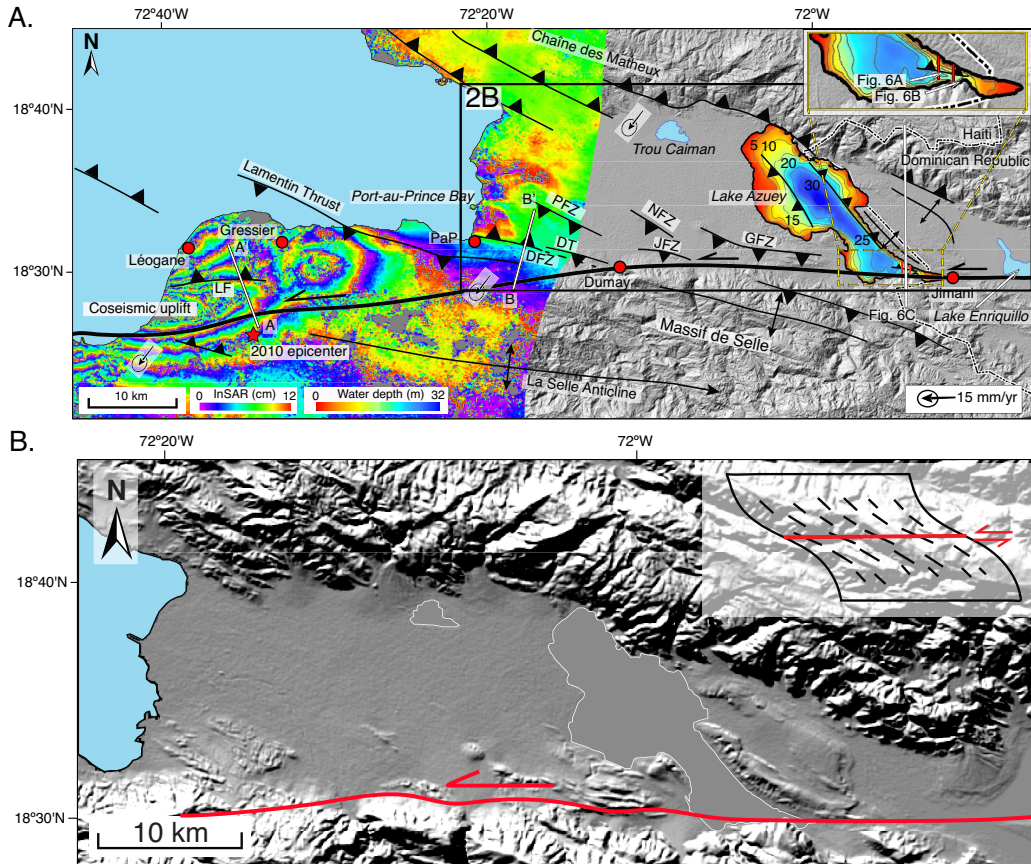
- 794 Mann, P., E. Calais, J.-C. Ruegg, C. DeMets, P. E. Jansma, and G. S. Mattioli (2002),
795 Oblique collision in the northeastern Caribbean from GPS measurements and geological
796 observations, *Tectonics*, 21(6).
- 797 Marshall, G. A., R. S. Stein, and W. Thatcher (1991), Faulting geometry and slip from co-
798 seismic elevation changes: the 18 October 1989, Loma Prieta, California, earthquake,
799 *Bulletin of the Seismological Society of America*, 81(5), 1660–1693.
- 800 Massoni, P. (1955), *Haiti: reine des Antilles*, Nouvelles Editions Latines.
- 801 McHugh, C. M., L. Seeber, N. Braudy, M.-H. Cormier, M. B. Davis, J. B. Diebold,
802 N. Dieudonne, R. Douilly, S. P. Gulick, M. J. Hornbach, et al. (2011), Offshore sedimentary effects of the 12 January 2010 Haiti earthquake, *Geology*, 39(8), 723–726.
- 803 Mercier de Lépinay, B., A. Deschamps, F. Klingelhoefer, Y. Mazabraud, B. Delouis,
804 V. Clouard, Y. Hello, J. Crozon, B. Marcaillou, D. Graindorge, et al. (2011), The 2010
805 Haiti earthquake: A complex fault pattern constrained by seismologic and tectonic ob-
806 servations, *Geophysical Research Letters*, 38(22).
- 807 Moknatian, M., M. Piasecki, and J. Gonzalez (2017), Development of Geospatial and
808 Temporal Characteristics for Hispaniola's Lake Azuei and Enriquillo Using Landsat
809 Imagery, *Remote Sensing*, 9(6), 510.
- 810 Nettles, M., and V. Hjörleifsdóttir (2010), Earthquake source parameters for the 2010 Jan-
811 uary Haiti main shock and aftershock sequence, *Geophysical Journal International*,
812 183(1), 375–380.
- 813 Odonne, F., and P. Vialon (1983), Analogue models of folds above a wrench fault,
814 *Tectonophysics*, 99(1), 31–46.
- 815 Olson, J. A. (1990), Seismicity in the twenty years preceding the loma prieta california
816 earthquake, *Geophysical Research Letters*, 17(9), 1429–1432.
- 817 Paultre, P., É. Calais, J. Proulx, C. Prépetit, and S. Ambroise (2013), Damage to engi-
818 neered structures during the 12 January 2010, Haiti (Léogâne) earthquake, *Canadian*
819 *Journal of Civil Engineering*, 40(8), 777–790.
- 820 Piasecki, M., M. Moknatian, F. Moshary, J. Cleto, Y. Leon, J. Gonzalez, and D. Co-
821 marazamy (2016), Report: Bathymetric Survey for Lakes Azuei and Enriquillo, His-
822 paniola, *Tech. rep.*, City University of New York (CUNY).
- 823 Prentice, C., P. Mann, A. Crone, R. Gold, K. Hudnut, R. Briggs, R. Koehler, and P. Jean
824 (2010), Seismic hazard of the Enriquillo-Plantain Garden fault in Haiti inferred from
825 palaeoseismology, *Nature Geoscience*, 3(11), 789–793.

- 827 Prentice, C. S., P. Mann, F. Taylor, G. Burr, and S. Valastro (1993), Paleoseismicity of
828 the north american-caribbean plate boundary (septentrional fault), dominican republic,
829 *Geology*, 21(1), 49–52.
- 830 Pubellier, M., A. Mauffret, S. Leroy, J. M. Vila, and H. Amilcar (2000), Plate boundary
831 readjustment in oblique convergence: Example of the Neogene of Hispaniola, Greater
832 Antilles, *Tectonics*, 19(4), 630–648.
- 833 Rathje, E., J. Bachhuber, B. Cox, J. French, R. Green, S. Olson, G. Rix, D. Wells, O. Sun-
834 car, E. Harp, et al. (2014), Geotechnical reconnaissance of the 2010 Haiti earthquake:
835 GEER (Geotechnical Extreme Events Reconnaissance).
- 836 Rico, P. (2017), Hydrodynamic Study of Lake Enriquillo in Dominican Republic, *Journal*
837 *of Geoscience and Environment Protection*, 5, 115–124.
- 838 Rios, J., C. McHugh, M. Hornbach, P. Mann, V. Wright, and D. Gurung (2013), Holocene
839 activity of the Enriquillo-Plantain Garden Fault in Lake Enriquillo derived from seismic
840 stratigraphy, in *AGU Fall Meeting Abstracts*, vol. 1, p. 2629.
- 841 Saint Fleur, N., N. Feuillet, R. Grandin, E. Jacques, J. Weil-Accardo, and Y. Klinger
842 (2015), Seismotectonics of southern Haiti: A new faulting model for the 12 January
843 2010 M7. 0 earthquake, *Geophysical Research Letters*, 42(23).
- 844 Segall, P., and M. Lisowski (1990), Surface displacements in the 1906 San Francisco and
845 1989 Loma Prieta earthquakes, *Science*, 250(4985), 1241–1244.
- 846 Sibson, R. (2012), Reverse fault rupturing: competition between non-optimal and optimal
847 fault orientations, *Geological Society, London, Special Publications*, 367(1), 39–50.
- 848 Sylvester, A. G. (1988), Strike-slip faults, *Geological Society of America Bulletin*, 100(11),
849 1666–1703.
- 850 Symithe, S., and E. Calais (2016), Present-day shortening in Southern Haiti from GPS
851 measurements and implications for seismic hazard, *Tectonophysics*, 679, 117–124.
- 852 Symithe, S. J., E. Calais, J. S. Haase, A. M. Freed, and R. Douilly (2013), Coseismic slip
853 distribution of the 2010 M 7.0 Haiti earthquake and resulting stress changes on regional
854 faults, *Bulletin of the Seismological Society of America*, 103(4), 2326–2343.
- 855 Taylor, F., P. Mann, S. Valastro Jr, and K. Burke (1985), Stratigraphy and radiocarbon
856 chronology of a subaerially exposed Holocene coral reef, Dominican Republic, *The*
857 *Journal of Geology*, 93(3), 311–332.
- 858 Terrier, M., A. Bialkowski, A. Nachbaur, C. Prépetit, and Y. Joseph (2014), Revision of
859 the geological context of the port-au-prince metropolitan area, haiti: implications for

- 860 slope failures and seismic hazard assessment, *Natural Hazards and Earth System Sci-*
861 *ences*, 14(9), 2577.
- 862 UNAVCO (University Navstar Consortium) (2009), PBO GPS velocities in southern Cali-
863 fornia.
- 864 Wright, V. D., M. J. Hornbach, C. Mchugh, and P. Mann (2015), Factors contributing to
865 the 2005-present, rapid rise in lake levels, dominican republic and haiti (hispaniola),
866 *Natural Resources*, 6(08), 465.

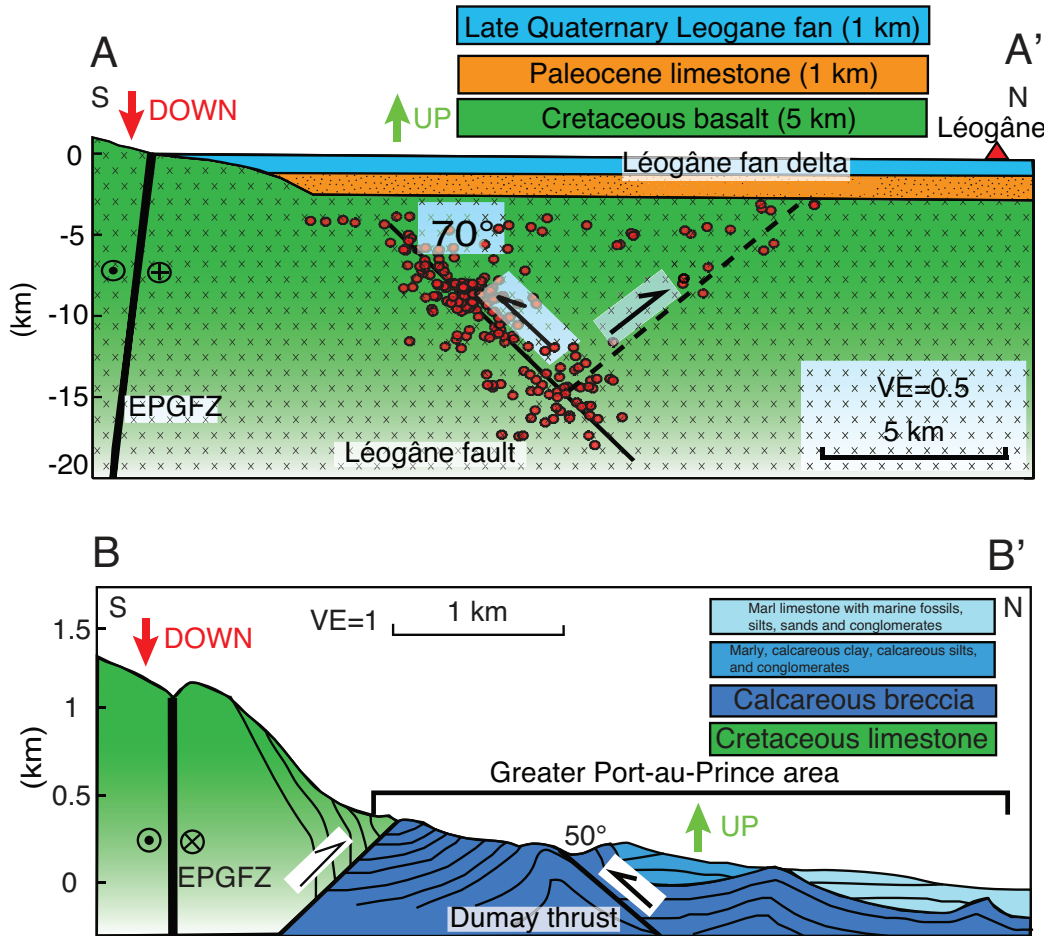


867 **Figure 1. Tectonic setting of the northeastern Caribbean and EPGFZ in southern Haiti. A:** Free-air
 868 gravity anomaly map of the Greater Antilles (Cuba, Jamaica, Hispaniola, Puerto Rico) in the northeastern
 869 Caribbean (<http://topex.ucsd.edu>) with gravity lows marking zones of subduction or thrusting along major
 870 faults (black lines) of the North America-Caribbean plate boundary. Arrows with error ellipses from *Calais*
 871 *et al.* [2010] are GPS vectors showing the direction and velocity of the large North American plate, the Ba-
 872 hamas **carbonate**-platform (**BP**), and intervening microplates relative to a fixed Caribbean plate. Microplates
 873 with variable relative motions occupy the 200 km-wide plate boundary zone and include: **NHM** = North His-
 874 paniola microplate; **HM** = Hispaniola microplate; **GM** = Gonâve microplate; **PRVIM** = Puerto Rico-Virgin
 875 Islands microplate. Box shows more detailed map of the EPGFZ shown in B. **B:** Regional structure map of
 876 the southern peninsula of Haiti with the active, left-lateral Enriquillo-Plantain Garden fault zone (EPGFZ)
 877 from the **Cul-de-Sac-Enriquillo basin-Lake Enriquillo** in the east to the **eastern-western** tip of the southern
 878 peninsula. **The centroid moment tensor (CMT) mechanism is from Douilly *et al.* [2013].** From east to west,
 879 key lakes and marine embayments aligned parallel and overlying the EPGFZ include: **LE** = Lake Enriquillo,
 880 Dominican Republic; **LA** = Lake Azuey, Haiti; **PAP PAPB** = Port-au-Prince Bay; **CS** = Canal du Sud; and
 881 **LA LM** = Lake Miragoâne; **LF** = **Léogâne fault**. Boxes shows more detailed maps of the structure of the
 882 EPGFZ and its secondary faults shown in Figure 2A and Figure 3A. **C:** Composite, multichannel seismic
 883 reflection line **from** **(acquired by)** Canadian Superior **Energy Inc.** located as the red line X-X' in B that shows
 884 an unfolded area of high-angle faults in the Canal du Sud tied to the offshore Cul-de-Sac-1 well, the TBFZ,
 885 the EPGFZ, the anticlinal structure of the southern peninsula, and a large, south-verging accretionary prism
 886 along the south coast of the southern peninsula. The depth scale for this section is in two-way, travel time.



887 **Figure 2. Structure of the EPGFZ in eastern Haiti. A:** Geologic faults and folds along a 15 km-wide
 888 corridor parallel to the EPGFZ superimposed on a modified DEM and InSAR surface deformation map
 889 [Hayes *et al.*, 2010; Hashimoto *et al.*, 2011]. Chirp bathymetry of the Lake Azuey is also shown. GPS vectors
 890 are from Calais *et al.* [2010]. **PaP-T PFZ** = Port-au-Prince thrustfault zone; **DFZ** = Dumay fault zone; **DT**
 891 = Dumay thrust; **NaC** = Nan Cadastre thrust; **Jae JFZ** = Jacquet thrustfault zone; **Gant-T GFZ** = Ganthier
 892 thrustfault zone; **LF** = Léogâne fault. **Line A – A'**: Cross-section along the blind Léogâne thrust fault (shown
 893 in Figure 3); **Line B – B'**: Cross-section of north Port-au-Prince urban area (shown in Figure 3). **B:** Shaded
 894 DEM of the northern deformed belt in the Cul-de-Sac basin with illumination from the Figure 2A showing
 895 en echelon and curvilinear folds extending from north-northwest from striking west-northwest obliquely with
 896 respect to the EPGFZ and plunging beneath undeformed sediments occupying the center of the Cul-de-Sac
 897 Valley. The inserted schematic diagram is from Odonne and Vialon [1983].

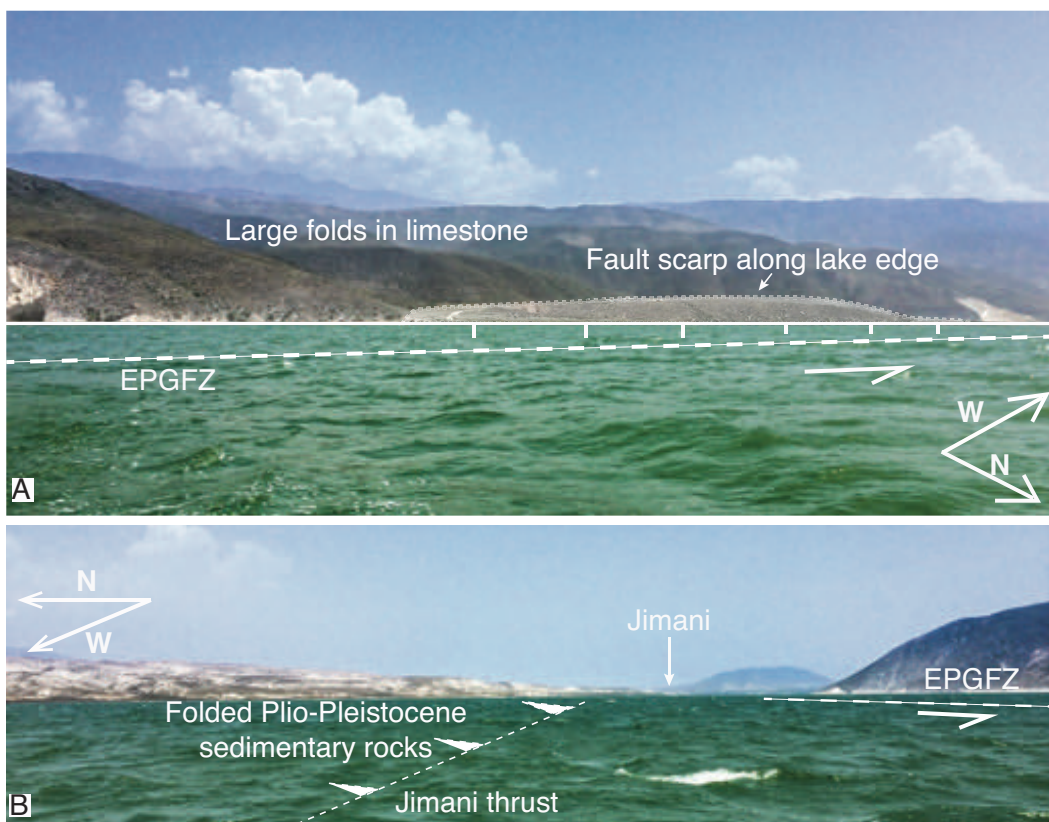
~



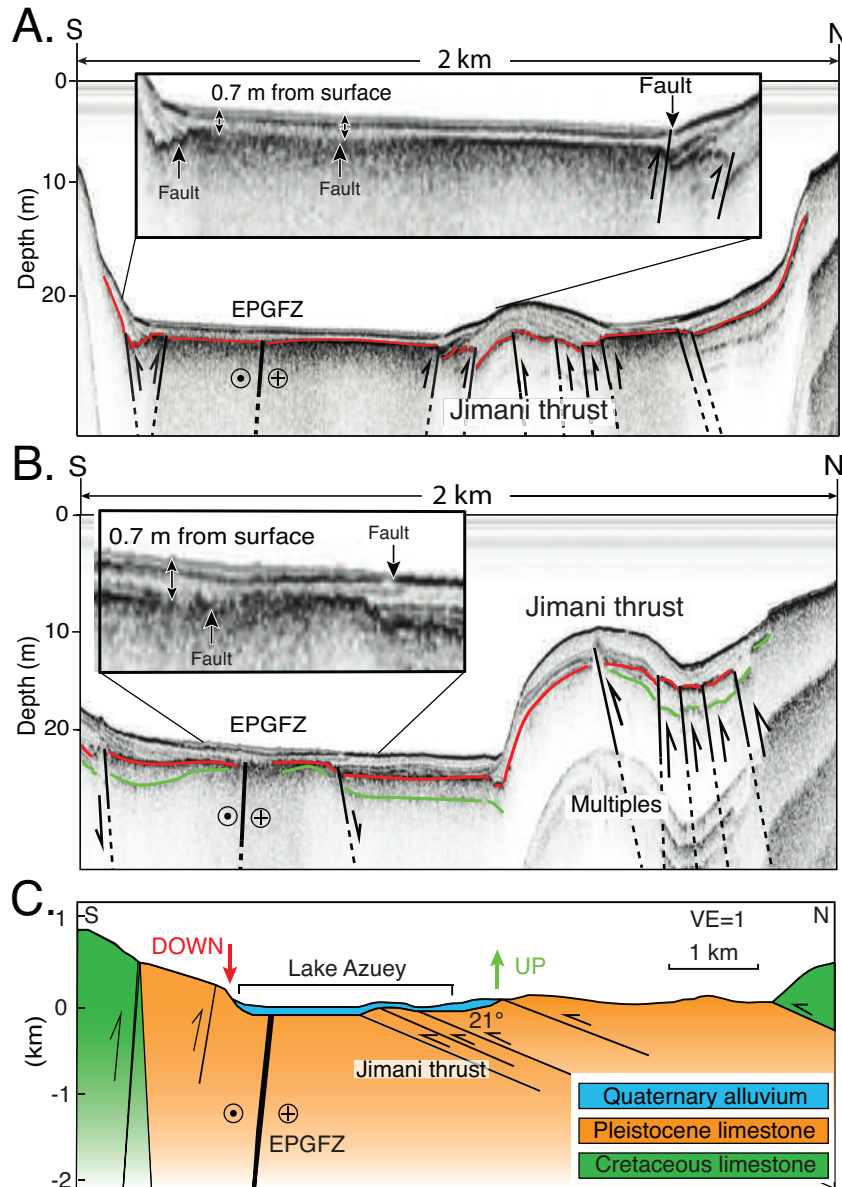
898 **Figure 3. Style of late Neogene deformation in the northern belt along three transects shown on the**
 899 **map in Figure 2. Style of late Neogene deformation in the northern belt along three transects shown in**
 900 **Figure 2. A-A':** Aftershocks of the 2010 earthquake [Douilly *et al.*, 2013] along the blind Léogâne thrust fault
 901 reveals conjugate reverse faults with the dominant slip occurring on the north-dipping fault. **The red triangle**
 902 **indicates Léogâne city.** **B-B':** Cross section based on surface mapping [Massoni, 1955; Cox *et al.*, 2011;
 903 *McHugh et al.*, 2011; Saint Fleur *et al.*, 2015] showing north- and south-dipping reverse faults deforming
 904 Plio-Pleistocene sedimentary rocks. **C-C':** Cross section based on both sonar survey and the surface mapping
 905 showing north- and south-dipping, reverse faults deforming Plio-Pleistocene sedimentary rocks.

Structure of the EPGFZ in eastern Haiti and western-most Dominican Republic. A:

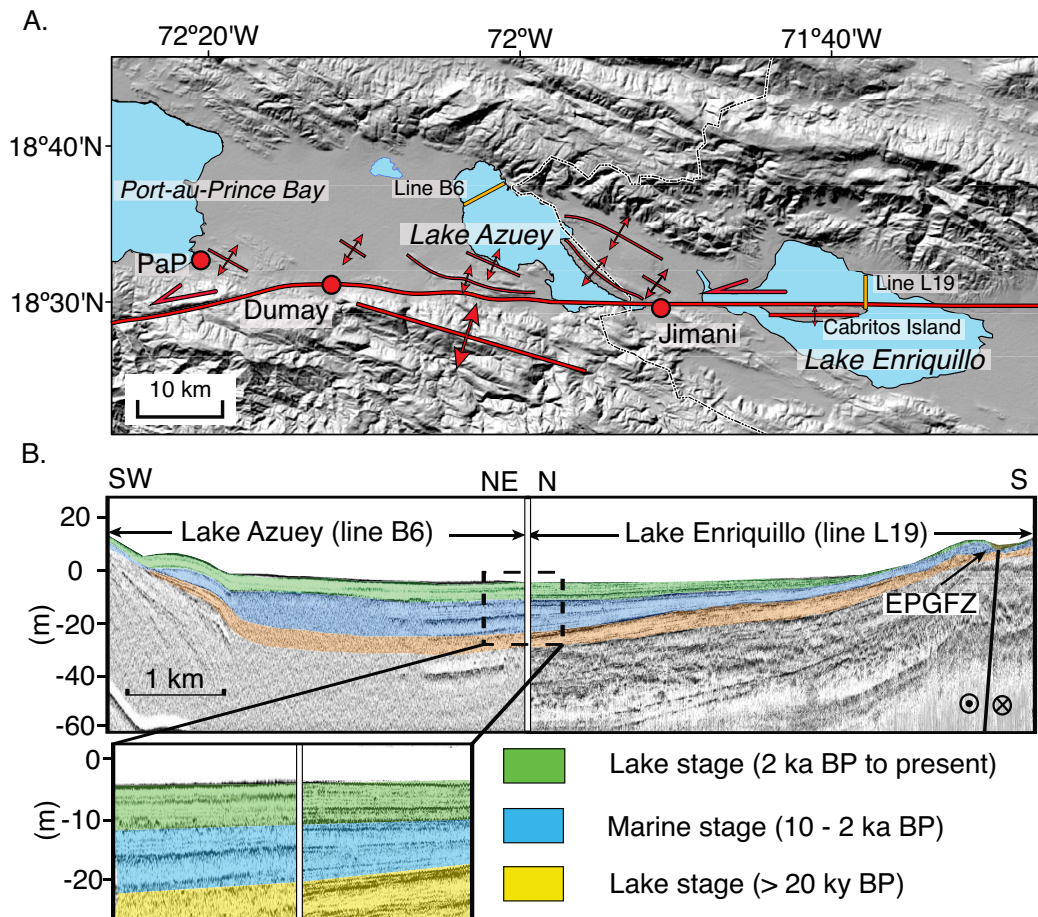
Structural map of Lakes Azuey and Lake Enriquillo with surfaces of 15 m ASL and 46 m BSL are presently separated by a shallow sill 30 m ASL in the isthmus near the town of Jimani. **B:** Comparison of two Chirp lines from Lake Enriquillo by (3 km-long Line L19) and from this own study of Lake Azuey (4 km-long Line B6). Identical sequences present on both lines suggest that the two lakes were once part of a single lake that has been recently separated by crustal movements related to the EPGFZ near the Jimani area. Ages of units are known from Lake Enriquillo through both exposures around the sub-sea level lake and from coring by.



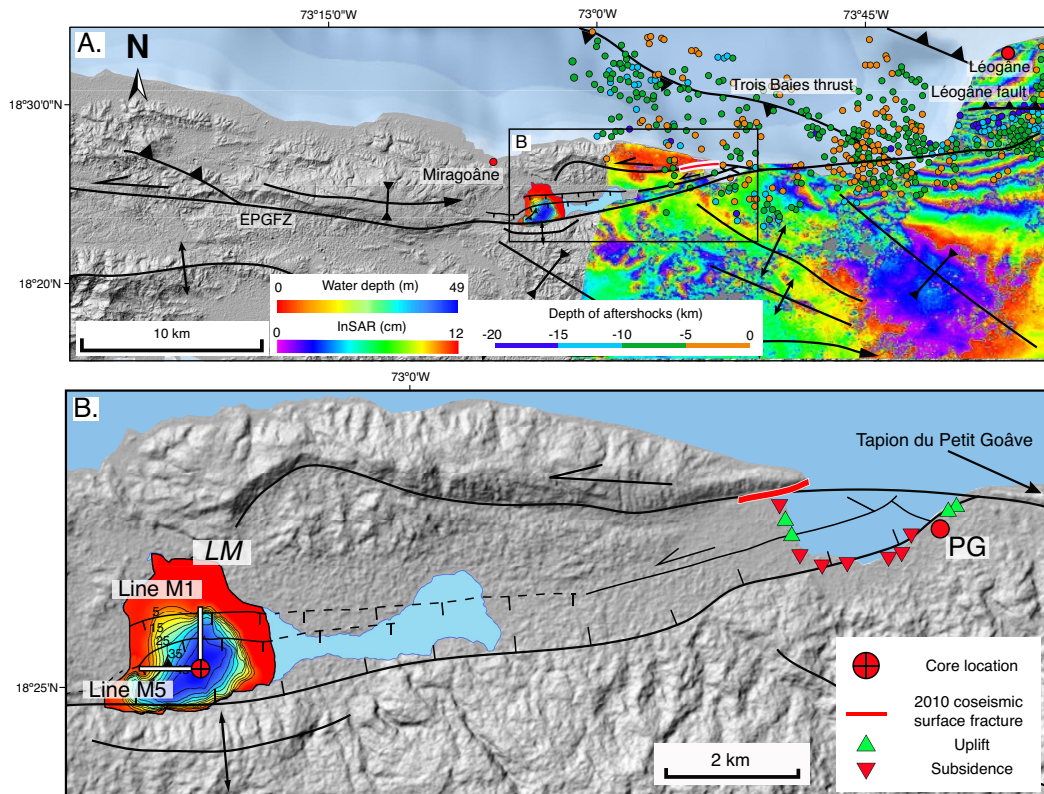
906 **Figure 4. Geologic setting of Lake Azuey, Haiti. A:** To the south, the green brackish waters of Lake
 907 Azuey are bound by the EPGFZ which forms a sharp boundary with 2 km-high, folded limestone of Paleo-
 908 gene age that forms the smooth surfaces on the skyline. One scarp is present along the edge of the lake while
 909 other parallel strands of the EPGFZ are beneath the southern part of the lake as schematically shown. **B:** To
 910 the north of the lake folded, Plio-Pleistocene strata form the uplifted, 0 – 30 m-high isthmus separating the
 911 two lakes. Approximate locations of the EPGFZ and the Jimani thrust fault are shown.



912 **Figure 5.** Chirp sonar profiles showing the relationship of the trace of the EPGFZ and a newly de-
 913 scribed thrust we have named the **Jimani thrust**. Cross sections of A, and B are indicated in Figure 2A.
 914 The EPGFZ beneath Lake Azuey forms a 10 m-wide zone that can be traced as a lineament to the east and
 915 west of Lake Azuey (Figure 2). The green and red horizons represent two distinguish stratigraphic layers.
 916 The two strands of the EPGFZ are buried by 0.7 m of Holocene sediment and are extrapolated to be **250**
 917 **270** years old since their last rupture when a sedimentation rate of 2.6 mm/yr is assumed. Folds associate
 918 with the Jimani thrust are interpreted as fault propagation folds. **C:** Cross section based on both sonar survey
 919 and the surface mapping [Mann *et al.*, 1991] showing north- and south-dipping, reverse faults deforming
 920 Plio-Pleistocene sedimentary rocks.



921 **Figure 6. Structure of the EPGFZ in eastern Haiti and western-most Dominican Republic. A:**
922 Structural map of Lakes Azuey (surface 15 m ASL) and Lake Enriquillo (surface 46 m BSL) are presently
923 separated by a shallow sill 30 m ASL in the isthmus near the town of Jimani. **B:** Comparison of two Chirp
924 lines from Lake Enriquillo by Rios *et al.* [2013] (3 km-long Line L19) and from our study of Lake Azuey (4
925 km-long Line B6). Identical sequences present on both lines suggest that the two lakes were once part of a
926 single lake that has been recently separated by crustal movements related to the EPGFZ near the Jimani area.
927 Ages of units are known from Lake Enriquillo through both exposures around the sub-sea level lake and from
928 coring by Rios *et al.* [2013].



929 **Figure 7. Structure and 2010 coseismic surface deformation of the western segments of the EPGFZ.**

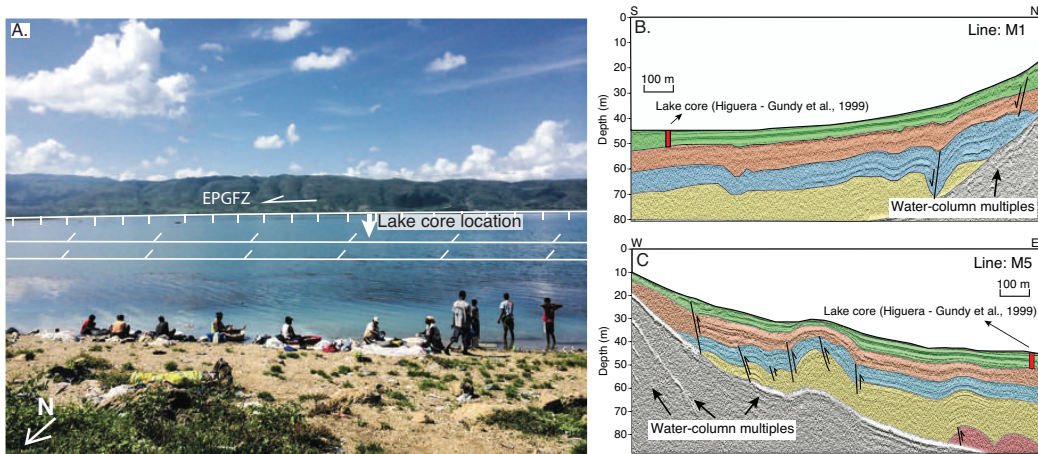
930 **A:** Structure [Prentice et al., 2010; Cowgill et al., 2012] and aftershock [Douilly et al., 2013] map of

931 Miragoâne-Léogâne region overlain with an InSAR image [Hashimoto et al., 2011]. **B:** Zoom of the area

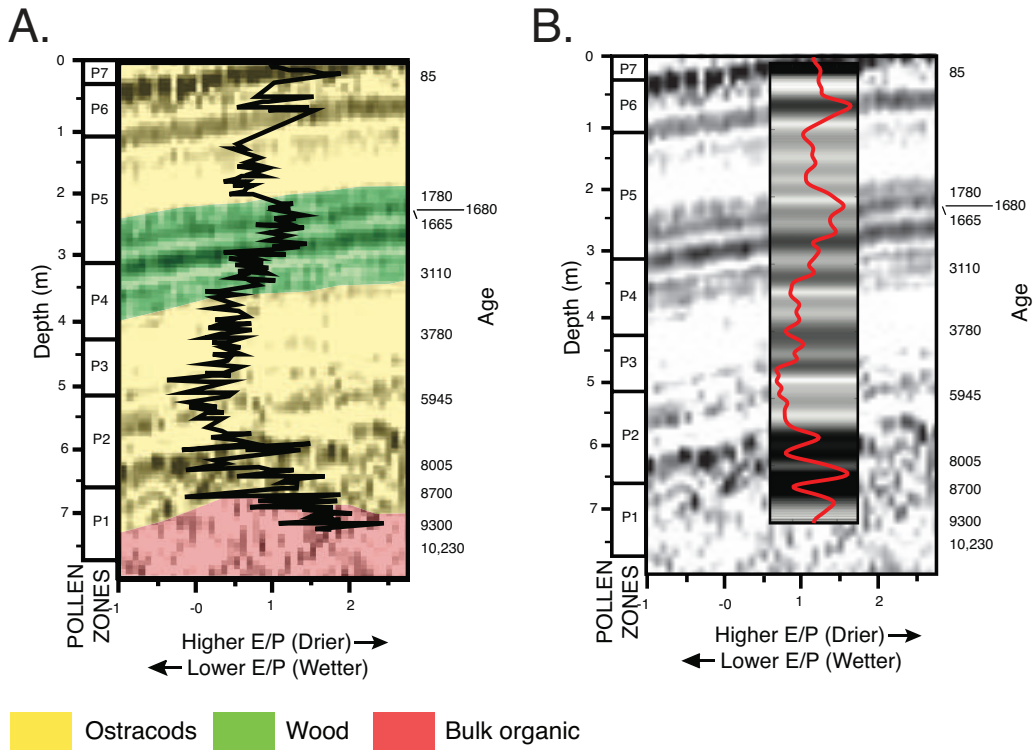
932 of Petit Goave and Lake Miragoâne showing the structure and bathymetry of the 14 km^2 , pull-apart basin

933 mapped beneath Lake Miragoâne during this study and details of the 2010 surface fracturing and coseismic

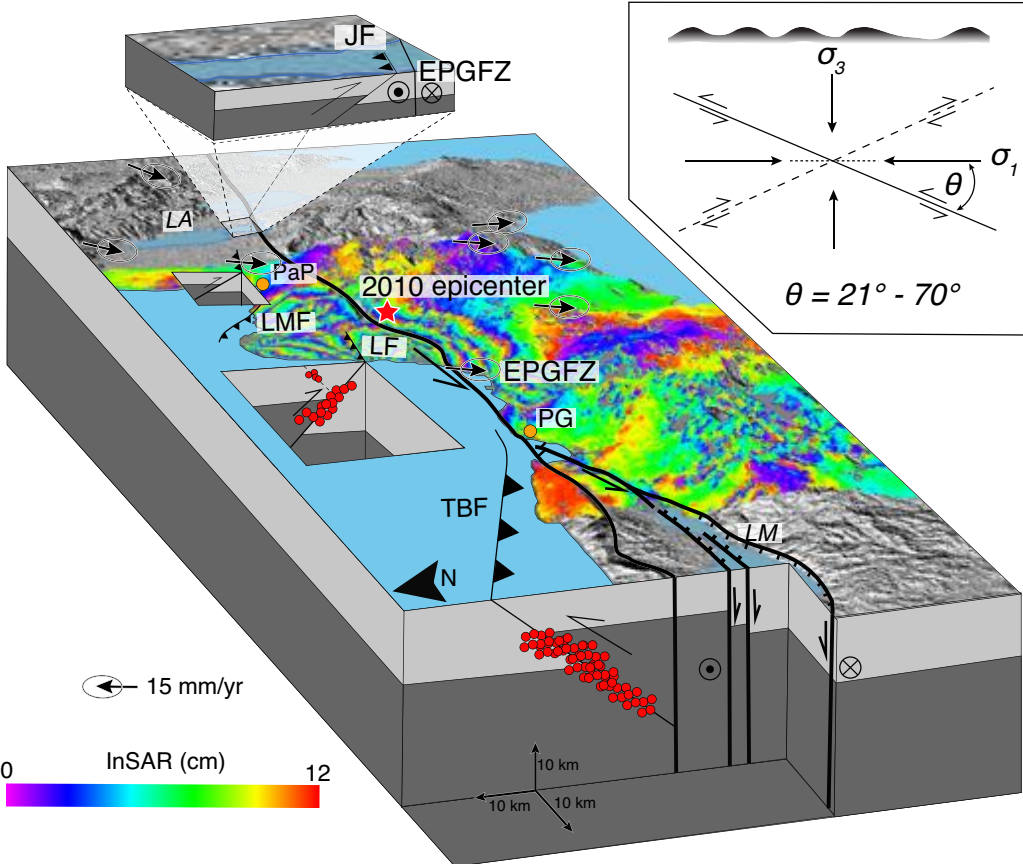
934 subsidence in the Petit Goâve Bay [Prentice et al., 2010]. **LM** = Lake Miragoâne; **PG** = Petit Goâve.



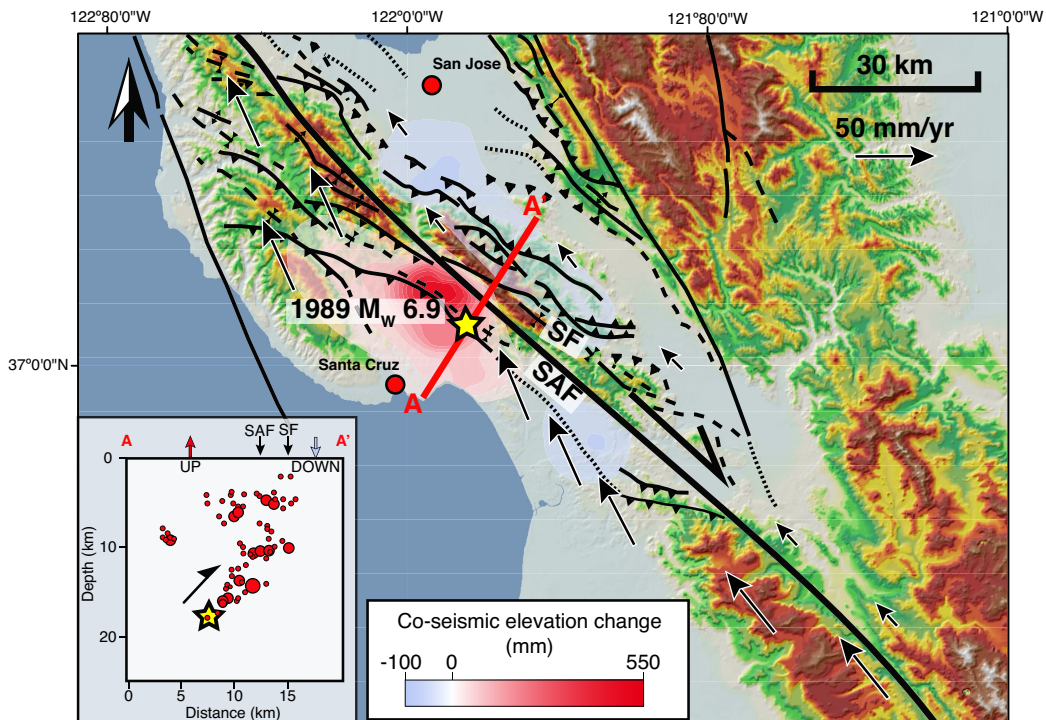
935 **Figure 8. Geologic setting and sonar profiles from Lake Miragoâne.** **A:** View looking south across the
 936 12 km-wide and 42.8 m deep, freshwater lake. The 2 km-high, ridge along the southern edge of the lake is
 937 the cumulative topographic scarp ofassociated to the southernmost strand of the EPGFZ. The northern strand
 938 of the EPGFZ is 3 km to the north of this strand and forms the northern edge of the pull-apart basin. The
 939 core was taken by Higuera-Gundy et al. [1999] and was not collected from the deepest part of the lake. **B:**
 940 **C:** North-south trending line M1 (location shown on Figure 7B). **C:** East-west trending line M5 (location shown
 941 on Figure 7B).



942 **Figure 9. Core data from Lake Miragoâne. A:** Tie between chirp sonar and core [Higuera-Gundy *et al.*,
943 1999] extending to lacustrine sediments deformed by the EPGFZ at 1770 in 1770 A.D.. **B:** Low-pass filtered
944 E/P log (red) and the synthetic sonar profile generated from the low-pass filtered E/P log used as an acoustic
945 impedance. Red bar The chirp sonar profiles are from the location of the red bars in the Figure 8A, B is the
946 core measurement location C.



947 **Figure 10.** Three-dimensional block diagram showing the structural and aftershock expression of
 948 late Holocene strain partitioning in a 40-km-wide zone along a 120 km-long segment of the EPGFZ.
 949 Three-dimensional block diagram showing the structural, aftershocks, and the late Holocene strain
 950 partitioning in a 40-km-wide zone along a 120 km-long segment of the EPGFZ. Black arrows show south-
 951 west direction of the Gonâve microplate relative to the Caribbean plate and [Calais et al., 2010]. The 2010
 952 InSAR-derived surface deformation map show and a large component of shortening accommodated on a 40
 953 km-wide zone of oblique thrusts and folds north of the EPGFZ. PaP = Port-au-Prince; PG = Petit Goave; LA
 954 = Lake Azuey; LM = Lake Miragoâne-Léogâne; JF = Jimani thrust fault; LMF = Lamartin thrust fault; TBF
 955 = Trois Baies thrust fault; LF = Léogâne fault. The inserted schematic diagram, modified from Sibson [2012],
 956 represents the conjugate thrust faults.



957 **Figure 11. Structural map of the San Francisco Bay region, the coseismic elevation and the**
 958 **aftershock cross-section of 1989 M_w 6.9 Loma Prieta earthquake. Structural map of the southern San**
 959 **Francisco Bay region, the coseismic elevation and the aftershock cross-section of 1989 M_w 6.9 Loma**
 960 **Prieta earthquake. The selected GPS vectors relative to a fixed North America plate are from UNAVCO**
 961 **(University Navstar Consortium) [2009]. The coseismic elevation change and aftershock cross-section are**
 962 **modified from Marshall *et al.* [1991]. SAF: San Andreas Fault; SF: Sargent Fault.**